Geosphere

Three-dimensional magma flow dynamics within sub-volcanic sheet intrusions

--Manuscript Draft--

Manuscript Number:	GS1270R2
Full Title:	Three-dimensional magma flow dynamics within sub-volcanic sheet intrusions
Short Title:	Magma flow dynamics in sheet intrusions
Article Type:	Research Paper
Keywords:	Anisotropy of magnetic susceptibility; inclined sheet; Ardnamurchan; magma flow; titanomagnetite; intrusion
Corresponding Author:	Craig Magee Imperial College London, London UNITED KINGDOM
Corresponding Author Secondary Information:	
Corresponding Author's Institution:	Imperial College
Corresponding Author's Secondary Institution:	
First Author:	Craig Magee
First Author Secondary Information:	
Order of Authors:	Craig Magee
	Brian O'Driscoll
	Michael S Petronis
	Carl TE Stevenson
Order of Authors Secondary Information:	
Abstract:	Sheet intrusions represent important magma conduits and reservoirs in sub-volcanic systems. Constraining the emplacement mechanisms of such intrusions is crucial to understanding the physiochemical evolution of magma, volcano deformation patterns, and the location of future eruption sites. However, magma plumbing systems of active volcanoes cannot be directly accessed and we therefore rely on the analysis of ancient systems to inform the interpretation of indirect geophysical and geochemical volcano monitoring techniques. Numerous studies have demonstrated that anisotropy of magnetic susceptibility (AMS) is a powerful tool for constraining magma flow patterns within such ancient, solidified sheet intrusions. Here, we conduct a high-resolution AMS study of seven inclined sheets, exposed along the Ardnamurchan peninsula in NW Scotland, and examine how magma flow in sheet intrusions may vary along and perpendicular to the magma flow axis. The sheets form part of the Ardnamurchan Central Complex, which represents the deeply eroded roots of a ~58 Myr old volcano. Our results suggest that the inclined sheets were emplaced via either up-dip magma flow or along-strike, lateral magma transport. Importantly, observed variations in magnetic fabric orientation, particularly magnetic foliations, within individual intrusions suggests that some sheets were internally compartmentalized; i.e. different along-strike portions of the inclined sheets exhibit subtle differences in their magma flow dynamics. This may have implications for the flow regime and magma mixing within intrusions.

Three-dimensional magma flow dynamics within sub-volcanic sheet intrusions

C. MAGEE*[1], B. O'DRISCOLL[2, 3], M.S. PETRONIS[4], C.T.E. STEVENSON[5]

[1]Basins Research Group (BRG), Department of Earth Sciences and Engineering, Imperial College, London, SW7 2BP, UK

[2]School of Physical and Geographical Sciences, Keele University, Keele, ST5 5BG, UK

[3]Now at: School of Earth, Atmospheric and Environmental Sciences, University of Manchester, Williamson Building, Oxford Road, Manchester M13 9PL, UK

[4]Environmental Geology, Natural Resource Management Department, New Mexico Highlands University, PO Box 9000, Las Vegas, NM 87701, USA

[5]School of Geography, Earth, and Environmental Sciences, University of Birmingham, Birmingham, B15 2TT, UK

Abstract

Sheet intrusions represent important magma conduits and reservoirs in sub-volcanic systems. Constraining the emplacement mechanisms of such intrusions is crucial to understanding the physiochemical evolution of magma, volcano deformation patterns, and the location of future eruption sites. However, magma plumbing systems of active volcanoes cannot be directly accessed and we therefore rely on the analysis of ancient systems to inform the interpretation of indirect geophysical and geochemical volcano monitoring techniques. Numerous studies have demonstrated that anisotropy of magnetic susceptibility (AMS) is a powerful tool for constraining magma flow patterns within such ancient, solidified sheet intrusions. Here, we conduct a high-resolution AMS study of seven inclined sheets, exposed along the Ardnamurchan peninsula in NW Scotland, and examine how magma flow in sheet intrusions may vary along and perpendicular to the magma flow axis. The sheets form part of the Ardnamurchan Central Complex, which represents the deeply eroded roots of a ~58 Myr old volcano. Our results suggest that the inclined sheets were emplaced via either up-dip magma flow or along-strike, lateral magma transport. Importantly, observed variations in magnetic fabric orientation, particularly magnetic foliations, within individual intrusions suggests that some sheets were internally compartmentalized; i.e. different along-strike portions of the inclined sheets exhibit subtle differences in their magma flow dynamics. This may have implications for the flow regime and magma mixing within intrusions.

Introduction

The transport of magma within a sub-volcanic system is commonly facilitated by interconnected sheet intrusions (e.g., dikes and sills). Because magma plumbing systems of active volcanoes cannot be directly observed, analyzing ancient sheet intrusion complexes exposed at the surface is crucial to understanding magma transport within sub-volcanic domains (e.g., Anderson 1937; Walker 1993; Schirnick et al. 1999; Gudmundsson 2002; Muirhead et al. 2012; Schofield et al. 2012b; Cashman and Sparks 2013; Petronis et al. 2013). Analyses of ancient sheet intrusion complexes provide invaluable insights into magma emplacement mechanisms and thereby contribute to volcanic hazard assessment (e.g., Sparks 2003; Sparks et al. 2012; Cashman and Sparks 2013), understanding the distribution of eruption locations (e.g., Abebe et al. 2007; Gaffney et al. 2007), and elucidating controls on crystal growth and geochemical variations (e.g., Latypov 2003). For example, studies of magma flow indicators (e.g., vesicle imbrication, phenocryst alignment, magnetic fabrics) in solidified intrusions have demonstrated that sheet geometries alone cannot be used as proxies for magma transport directions; i.e. flow within dikes or inclined sheets can range from dip-parallel to strike-parallel (e.g., Abelson et al. 2001; Holness and Humphreys 2003; Callot and Geoffroy 2004; Geshi 2005; Philpotts and Philpotts 2007; Kissel et al. 2010; Magee et al. 2012a). All studies focused on elucidating the structure and source of sub-volcanic intrusion complexes should therefore consider magma flow patterns.

Anisotropy of magnetic susceptibility (AMS) allows the rapid and precise measurement of magnetic fabrics from large sample sets (Tarling and Hrouda 1993). Numerous studies have successfully demonstrated that magnetic lineations and foliations, measured by AMS, can record information on primary magma flow in sheet intrusions (e.g., Fig. 1) (Launeau and Cruden 1998; Archanjo and Launeau 2004; Canon-Tapia and Chavez-Alvarez 2004; Féménias et al. 2004; Philpotts and Philpotts 2007; Stevenson et al. 2007b; Polteau et al. 2008; Petronis et al. 2013). For example, the imbrication of magnetic fabrics, which is related to increasing velocity gradients adjacent to the wall rock, can be used to establish magma flow directions (Fig. 1) (e.g., Knight and Walker 1988; Tauxe et al. 1998; Callot et al. 2001; Féménias et al. 2004). AMS therefore potentially provides a powerful tool for assessing magma flow in solidified sheet intrusions.

Although several studies have identified variations in magma flow-related AMS fabrics, particularly along strike of the principal emplacement direction in individual intrusions, the processes that generate local variations in magma flow dynamics remain poorly constrained (e.g., Ernst and Baragar 1992; Canon-Tapia and Chavez-Alvarez 2004; Aubourg et al. 2008; Cañón-Tapia and Herrero-Bervera 2009; Magee et al. 2013a). For example, Magee et al. (2013b) recently conducted an AMS analysis of numerous intrusions exposed in the Ardnamurchan Central Complex (NW Scotland), and identified that the magnetic fabric orientations measured occasionally varied along sheet strike. Assuming that the magnetic fabrics record lateral variations in the magma flow pattern, Magee et al. (2013b) speculated that individual inclined sheets were locally compartmentalized because rheological differences between adjacent magma pulses promoted the internal segmentation of otherwise continuous sheet intrusions. Importantly, the potential preservation of internal compartmentalization implies that mixing (e.g., chemical composition, crystal population transfer or xenolith transport) within continuous sheet intrusions may be laterally restricted and could result in the preferential channelization of magma (Holness and Humphreys 2003; Magee et al. 2013a). In this study, we present a high resolution AMS analysis combined with structural measurements and field observations of seven sheet intrusions within the Ardnamurchan

Central Complex. An important aim of this study is to assess how magnetic fabric variations that correspond to localized, intra-intrusion magma flow dynamics can be elucidated and distilled from overall magma flow patterns.

Geological Setting

The Ardnamurchan Central Complex is located in NW Scotland and comprises a suite of major intrusions (e.g., laccoliths and lopoliths) and numerous minor sheet intrusions (Fig. 2) (Emeleus and Bell 2005). This exposed magmatic network represents the deeply eroded roots of an ancient volcanic edifice that formed at ~58 Ma during the development of the British and Irish Paleogene Igneous Province (BIPIP) (Emeleus and Bell 2005). Intensive igneous activity at this time (~61–55 Ma) was fundamentally related to the incipient opening of the North Atlantic and associated lithospheric impingement of a mantle plume (Saunders et al. 1997).

Sheet intrusions in Ardnamurchan are primarily diabase, typically <1 m thick, and display a variety of orientations (Magee et al. 2012a). They were emplaced into a complex host rock stratigraphy on Ardnamurchan that consists of Neoproterozoic Moine Supergroup metasedimentary rocks (i.e. Upper Morar Group) unconformably overlain by Mesozoic metasedimentary strata (e.g., the calcareous Blue Lias Formation, interbedded limestones and shales of the Pabay Shale Formation and the Bearreraig Sandstone Formation) and Early Paleogene volcaniclastics and olivine-basalt lavas (Fig. 2) (Emeleus and Bell 2005; Emeleus 2009). The sheet intrusions predominantly display a concentric or arcuate strike (Fig. 2) and an inward inclination (Richey and Thomas 1930; Emeleus 2009). This apparent inverted conical geometry, also exhibited by similar intrusion suites within the Mull and Skye central complexes, forms the foundation of the cone sheet emplacement model developed by Bailey (1924) and Anderson (1936). The assumption that cone sheets and their host fractures can be simply projected down-dip to a convergence point has led to the notion that they are fed from a central, overpressured magma chamber (Bailey 1924; Richey and Thomas 1930; Anderson 1936). For example, Richey and Thomas (1930) used linear projections of the Ardnamurchan cone sheet dips and the location of the major intrusions to originally define three intrusive foci, which were inferred to reflect three spatially and temporally separate centers of magmatic activity (Fig. 2). However, numerous studies have re-evaluated the geometry and emplacement mechanisms of major intrusions on Ardnamurchan and have questioned this hypothesis (e.g., Day 1989; O'Driscoll et al. 2006; O'Driscoll 2007; Magee 2012; Magee et al. 2012b). Burchardt et al. (2013) have more recently constructed a 3D down-dip projection of the cone sheets and suggested that the principal zone of convergence corresponds to a ~6 × 5 km (elongated E-W), ellipsoidal source reservoir emplaced at 3.5–5 km depth (Fig. 2).

Magee et al. (2012a) presented an alternative interpretation for cone sheet emplacement based on an analysis of magma flow patterns, derived from magnetic fabrics. The sub-horizontal, strike-parallel flow fabrics identified in the majority of intrusions led to the proposal that the cone sheets represent laterally propagating regional dikes (i.e. externally sourced), which upon entering the vicinity of the Ardnamurchan Central Complex were deflected by the local stress field into pre-existing, inwardly inclined, concentric fractures (Magee et al. 2012a). Although Magee et al. (2012a) did not preclude the origin of some of the Ardnamurchan sheet intrusions originating from a central source, i.e. a prerequisite of the cone sheet model, the term ‘inclined sheet’ is henceforth utilized for all sheet intrusions studied in the present work in order to avoid genetic connotations (cf. Gautneb et al. 1989; Gautneb and Gudmundsson 1992; Siler and Karson 2009).

Methodology

Magnetic fabrics as a record of magma flow

Magma flow petrofabrics in sheet intrusions may be attributed to the hydrodynamic alignment of suspended crystal populations by non-coaxial shear or coaxial shear, dependent on variations in magma-velocity gradients across the intrusion (e.g., Fig. 1) (Correa-Gomes et al. 2001; Callot and Guichet 2003; Canon-Tapia and Chavez-Alvarez 2004). Although this hydrodynamic alignment is typically considered to be stable during magma flow (i.e. crystal orientations remain fixed once aligned), experimental work suggests that this assumption is only valid if the crystal content is >20 % because collisions prevent crystal rotation (see Cañón-Tapia and Herrero-Bervera 2009 and references therein). Below this threshold, crystals within a flowing magma display a cyclic behavior, whereby the rotation of their principal axes means that the crystals transition between flow parallel and non-parallel orientations (Canon-Tapia and Chavez-Alvarez 2004; Cañón-Tapia and Herrero-Bervera 2009). The time each crystal spends in either stage of the cyclic phase (i.e. flow parallel or non-parallel) is controlled by the aspect ratio of the crystal and the amount of shear; e.g., high aspect ratio phenocrysts spend the majority of time in a flow parallel orientation (Cañón-Tapia and Herrero-Bervera 2009). These theoretical considerations of crystal cyclicity therefore imply that if a significant proportion of crystals are non-parallel to flow in a specific part of an intrusion during solidification, then the average petrofabric of a corresponding sample may not obviously relate to the magma flow conditions (Canon-Tapia and Chavez-Alvarez 2004; Cañón-Tapia and Herrero-Bervera 2009). Magma flow within an intrusion can also vary with time, potentially producing a range of petrofabric orientations preserved in different zones of a sheet intrusion. For example, petrofabrics within chilled margins are likely to relate to the initial magma propagation conditions, whereas fabrics in thick sheet intrusion cores may correlate to a more mature phase of magma flow (e.g., backflow or convection; Philpotts and Philpotts 2007). Magma flow fabrics can also be overprinted by post-emplacement processes such as convection and tectonic compression (e.g., Borradaile and Henry 1997; Schulmann and Ježek 2012).

It is clear that petrofabrics preserved in sheet intrusions may have a complex origin and history. Anisotropy of magnetic susceptibility (AMS) provides a quantitative measure of mineral alignments (e.g., of titanomagnetite phenocrysts in mafic rocks) and is particularly useful for fine-grained rocks where petrofabrics may not be optically resolvable (Tarling and Hrouda 1993; Dunlop and Özdemir 2001). Even in weakly anisotropic material, it is now widely accepted that magnetic lineations and foliations commonly reflect the magmatic petrofabric, providing information on magma migration, flow geometries, and regional strain (King 1966; Owens and

Bamford 1976; Hrouda 1982; Borradaile 1987; Rochette 1987; Borradaile 1988; Tarling and Hrouda 1993; Borradaile and Henry 1997; Bouchez 1997; Sant'Ovaia et al. 2000; Petronis et al. 2004; Horsman et al. 2005; O'Driscoll 2006; Stevenson et al. 2007a; Petronis et al. 2009; Kratinova et al. 2010). In particular, numerous studies have substantiated the relationship between the orientation of magnetic minerals and magma flow through correlation with visible magma flow indicators (e.g., Callot et al. 2001; Aubourg et al. 2002; Liss et al. 2002; Horsman et al. 2005; Morgan et al. 2008). Knight and Walker (1988) presented an empirical study of AMS and suggested that the magnetic lineation could be equated to the primary magma flow axis. Furthermore, high magma velocity-gradients at sheet margins and crystal interactions have been shown to create imbricated fabrics, the closure direction of which coincides with the primary magma flow direction during initial emplacement (Fig. 1) (Tauxe et al. 1998; Correa-Gomes et al. 2001; Callot and Guichet 2003; Féménias et al. 2004; Philpotts and Philpotts 2007; Morgan et al. 2008). To interpret magma flow patterns from magnetic fabrics it is therefore important to: (i) sample different locations of an intrusion by collecting traverses of varying orientation, with respect to the sheet geometry, and analyzing multiple sites along sheet strike and/or dip (Cañón-Tapia and Herrero-Bervera 2009); (ii) independently determine magma flow patterns within sheet intrusions if possible (e.g., measuring visible magma flow indicators); and (iii) consider whether primary fabrics have been modified by later magmatic or tectonic processes.

AMS Technique

In this study, seven separate sheet intrusions (S1–S7) that intrude a variety of host rocks and display a range of orientations (i.e. sills to dikes) have been analyzed in the southern portion of the Ardnamurchan peninsula. Similar to the majority of inclined sheets on Ardnamurchan, the analyzed intrusions are aphyric and predominantly consist of fine- to medium-grained (<0.05–0.5 mm) plagioclase microlites, skeletal clinopyroxene, and titanomagnetite (Magee 2011; Magee et al. 2012a; Magee et al. 2013a). The relatively fine grainsize of the inclined sheets is challenging for petrological (petrographic) analyses of silicate fabrics. Of the seven inclined sheets examined, AMS fabrics have previously been analyzed for three intrusions (i.e. S2, S4, and S7) by Magee et al. (2012a); their analysis involved the collection of one (i.e. S2 and S4) or three (i.e. S7) block samples for each intrusion, a strategy that was not designed to investigate local magma flow pattern variations in individual intrusions. AMS samples used in this study were collected in 2008, typically from two or more sites along sheet strike, as oriented drill-cores using a portable gasoline powered drill with a non-magnetic diamond bit. All samples were oriented using a magnetic and (when possible) a sun compass. Depending on exposure quality, suites of samples were extracted at each site and binned into profiles characterizing the intrusions margins and core or an entire sheet-orthogonal traverse. This sampling strategy allows any lateral and vertical variations in the magnetic fabrics to be spatially analyzed.

The AMS fabrics of each specimen were measured on either an AGICO KLY-3S Kappabridge (an induction bridge that operates at a magnetic field of 300 A/m and a frequency of 875Hz) at the University of Birmingham (UK) (i.e. S1, S6 and S7) or on an AGICO MFK1-A (an induction bridge operating at 976 Hz with a 200 A/m applied field) at New Mexico Highlands University (USA) (i.e. S2–S5). Some S1, S6, and S7 specimens were remeasured on the AGICO MFK1-A and showed no difference in magnetic fabric results between the two induction bridges. Magnetic susceptibility differences were measured in three orthogonal planes and combined with one axial susceptibility measurement to define the susceptibility tensor. This tensor, which may be visualized as an ellipsoid, comprises the three principal susceptibility magnitudes ($K_1 \geq K_2 \geq K_3$) and a corresponding set of three orthogonal principal axis directions.

Where magnetic fabrics are prolate and the shape of the susceptibility ellipsoid is elongated along the K_1 axis, it is at times appropriate to interpret the orientation of the K_1 lineation in the context of a flow or stretching direction, although many caveats exist when interpreting the linear fabric (e.g., Ellwood 1982; Knight et al. 1986; Hillhouse and Wells 1991; Geoffroy et al. 1997; Le Pennec et al. 1998; Tauxe et al. 1998). Conversely, oblate fabrics correspond to a susceptibility ellipsoid that is flattened in the K_1-K_2 plane (e.g., Tarling and Hrouda 1993). Commonly, the orientation of the K_1-K_2 susceptibility axes varies between specimens from the same sample, with the overall dispersion of the two susceptibility axes defining a great-circle girdle on a stereographic projection. Therefore, if the fabric elements at a site are strongly oblate and the 95% confidence ellipses of the K_1 and K_2 axes overlap in the K_1-K_2 plane, it is often not appropriate to interpret the orientation of the K_1 lineation as a flow or stretching direction (e.g., Canon-Tapia 2004; Cañón-Tapia and Herrero-Bervera 2009).

The magnitude parameters are reported in terms of ‘size’, ‘shape’ and ‘strength’ (or ellipticity) of the ellipsoid. These include the mean (or bulk) susceptibility, $K_{mean} = (K_1 + K_2 + K_3)/3$; the degree of anisotropy ($P_j = \exp\sqrt{(2[(\eta_1 - \eta)^2 + (\eta_2 - \eta)^2 + (\eta_3 - \eta)^2])}$, where $\eta = (\eta_1 + \eta_2 + \eta_3)/3$, $\eta_1 = \ln K_1$, $\eta_2 = \ln K_2$, $\eta_3 = \ln K_3$; Jelínek, 1981) and the shape parameter ($T = [2\ln(K_2/K_3)/(\ln(K_1/K_3)] -1$). The latter parameters (P_j and T) are reported as dimensionless parameters, whereas K_{mean} is measured in SI units. A value of $P_j = 1$ describes a perfectly isotropic fabric, whilst a P_j value of 1.15, for example, corresponds to a sample with 15% anisotropy (P gives a value that translates directly to % anisotropy whereas Pj is a close approximation). The quantitative measure of the shape of the susceptibility ellipsoid (T), ranges from perfectly oblate ($T = +1$) to perfectly prolate ($T = -1$).

Mineralogical controls on magnetic fabric orientation

Magnetic fabrics measured in titanomagnetite-bearing rocks are at times difficult to interpret because: (i) the relationship between the magnetite fabric and the mineral fabrics of the volumetrically dominant silicate phases is often uncertain; and (ii) titanomagnetite is frequently a relatively low-temperature liquidus phase. Importantly, quantitative textural analyses have demonstrated that titanomagnetite shape and distribution (i.e. its petrofabric) is commonly controlled by the primary silicate framework (e.g., Cruden and Launeau 1994; Launeau and Cruden 1998; Archanjo and Launeau 2004; O'Driscoll et al. 2008). The magnetic response of titanomagnetite is additionally controlled by grainsize as well as its shape anisotropy (Tarling and Hrouda 1993). Multi-domain (MD) titanomagnetites (>100 µm) have a strong shape-preferred anisotropy and thus their magnetic lineation will parallel the long axis of the grain. In contrast, single-domain (SD) magnetites (<1 µm) are more susceptible to magnetization along the magnetocrystalline 'easy' axis, orthogonal to the shape long axis (Hrouda 1982; O'Reilly 1984; Potter and Stephenson 1988; Dunlop and Özdemir 2001). From the dependence of principal susceptibility axis orientation on grainsize, titanomagnetite populations consisting purely of MD or SD grainsizes are interpreted to produce normal or inverse magnetic fabrics, respectively (Rochette et al. 1999; Ferré 2002). A normal magnetic fabric implies that the magnetic fabric mimics the mineral shape fabric, regardless of the fabric origin. Inverse magnetic fabrics are characterized by a K_1 and K_3 principal susceptibility axes that parallel the pole to the mineral foliation and the mineral lineation, respectively, complicating their interpretation somewhat. The term "inverse magnetic fabric" was originally coined by Rochette and Fillion (1988), who proposed that such fabrics may form in response to either: (i) c-axis preferred-orientation of ferroan calcite grains, whose maximum susceptibility is parallel to the c-axis; or (ii) the presence of single-domain (SD) elongated ferromagnetic grains. In magnetite or maghemite-bearing rocks, when the fabric is carried by SD grains, this leads to an inverse fabric (e.g., Potter and Stephenson 1988; Rochette and Fillion 1988; Borradaile and Puumala 1989). A mixture of SD and MD titanomagnetites may yield intermediate fabrics, where either one of or neither of the K_1 and K_3 principal susceptibility axes align with a component of the mineral shape fabric (Rochette et al. 1999; Ferré 2002).

When it can be demonstrated that the magnetic fabric is carried by paramagnetic ferromagnesian silicates, multidomian ferrimagnetic grains, or a mixture of both, it is commonly observed that the magnetic fabric and petrofabric agree. However, occasionally the petrofabric and magnetic fabric may still not coincide if there are magnetostatic interactions between individual, closely packed ferrimagnetic grains (Hargraves et al. 1991). These magnetostatic interactions can produce a distribution anisotropy, promoted by the generation of an asymmetric magnetic interaction field, which may contribute to the bulk magnetic anisotropy (Hargraves et al. 1991). Theoretical models have shown that when grains become closer and magnetostatically interact, the distribution of grains rather than their individual orientations dominate the petrofabric (e.g., Stephenson 1994; Grégoire et al. 1995; Cañón-Tapia 1996; Grégoire et al. 1998; Cañón-Tapia 2001).

To assess the magnetic mineralogy of the sheet intrusions in question in this study, high-temperature, low-field susceptibility experiments were conducted, using an AGICO MFK1-A (multi-function kappabridge) susceptibility meter and a CS4 furnace attachment, in a stepwise heating/cooling fashion from 25°C to 700°C to 40°C in an Ar atmosphere. Hysteresis measurements were conducted on a Lakeshore Shore Cryotronics MicroMag 2900/3900 Vibrating Sample Magnetometer (VSM) at the University of Texas-Dallas paleomagnetism laboratory. Hysteresis experiments involved vibrating the sample within a 3.0 T applied field at 83 Hz next to a set of pick-up coils. The vibrating sample creates a time varying magnetic flux in the coils, generating a current that is proportional to the sample's magnetization.

Results

This section presents the field observations and magnetic fabric analysis for each of the seven intrusions studied, as well as data pertaining to a suite of rock magnetic experiments. All orientation measurements are recorded as strike and dip unless otherwise stated. Magnetic data is presented in Table 1.

S1

Field observations

Diabase inclined sheets in the vicinity of S1 (UK National Grid co-ordinates NM 492 626; 56°41'16"N 6°05'45"W) display a wide range of orientations and locally complex intrusion morphologies (Figs 3 and 4) (see also Kuenen 1937; Magee et al. 2012a). The S1 intrusion is aphyric with grainsizes <2 mm; with the exception of a thin <1 cm chilled margin, no grainsize variation is observed across the inclined sheet at hand specimen scale. The ~1 m thick S1 intrusion (oriented 142/15° SW) is generally concordant to the local Blue Lias Formation bedding (~140/10° SW), except for a ~5 m wide zone where it transgresses stratigraphy at a steeper angle (018/55° SW) (Fig. 4a). This zone of transgression is bounded to the south by a ~35 cm thick inclined sheet (160/48° NE) that cross-cuts S1 (Fig. 4a). A steeply dipping dike (110/72° SW) impinges onto the base of the transgressive S1 portion, where it rotates into a sill (086/10° S) and exploits the contact between S1 and the host rock before terminating against the ~35 cm thick inclined sheet (Fig. 4a). Numerous studies have shown that such deflections of magmatic sheet intrusions may occur along boundaries that mark a significant contrast in the mechanical properties of the host rocks (e.g., Gudmundsson 2002; Kavanagh et al. 2006; Burchardt 2008; Gudmundsson 2011). The development of the inclined sheet into a sill may imply that its impingement locally uplifted S1. However, it is important to note that: (i) the sill is not observed on the southern side of an inclined sheet, which cross-cuts S1, suggesting that the sill terminated against a pre-existing intrusion; and (ii) adjacent bedding planes are not tilted (Fig. 4b). These observations indicate that the rotation of S1 is a primary, emplacement-related feature although the exact origins of such a perturbation in the sheet geometry remain unexplained and require further study.

Magnetic fabrics and susceptibilities

Two sites were sampled, separated by ~20 m, along the strike of S1. At each site, the base, middle, and top of S1 was sampled and a vertical traverse was also collected (Figs 3 and 4). The K_{mean} values (3.03×10^{-2} SI to 5.5×10^{-2} SI) of S1a-d describe a broad range whilst the P_j values range from 1.025–1.046 (Table 1). The T (-0.028 to -0.839) data reveal that the fabrics are triaxial to strongly prolate (Table 1). K_1 consistently trends NW-SE with plunges ranging from 3–29° (Fig. 3b; Table 1). Magnetic foliation strikes are within 10–23° of the inclined sheet strike (i.e. 129/18°

SW) but the base–middle sheet fabrics dip NE at 58–77° (Fig. 3b). Towards the top of the intrusion, the magnetic foliation dips SW at 9° and is sub-parallel to the orientation of the sheet (Fig. 3b).

The S1e-h samples are characterized magnetically by little variation in K_{mean} (6.16×10^{-2} to 6.91×10^{-2}), P_j (1.021–1.039), and magnetic fabrics that are triaxial (T = -0.069) to prolate (T = -0.619) (Figs 4b and c; Table 1). Although the magnetic lineations commonly plunge SE at ~21° (ranging from 3–45°), the orientation of the magnetic foliation varies with sample position (Figs 4b and d). Magnetic foliations from samples S1e and g, which correspond to the top and base of the intrusion respectively, lie close to the plane of intrusion (i.e. 142/15° SW) but dip in different directions; S1e strikes sub-parallel to the intrusion and dips at 20° SW whereas S1g dips SE at 14° (Figs 4b and d). In contrast to the two marginal samples of S1e and g, the girdle of K_2 sub-specimen axes in S1f (i.e. from the middle of S1) relative to the consistently oriented magnetic lineations, suggests that magnetic foliations within the sheet core are variable (Fig. 4b). This is supported by examining discrete sections of the vertical traverse, S1h. Towards the top of the intrusion, the magnetic foliations progressively rotate from sub-parallel to S1g (i.e. S1h_C) to steep, north-easterly dipping orientations (i.e. S1h_B and S1h_A are oriented at 165/54° NE and 130/73° NE, respectively) (Figs 4b and d; Table 1). S1h_B and S1h_A dip oppositely to the immediately overlying S1e fabric (Figs 4b and d). This change in orientation is coincident with a subtle increase in K_{mean} and change from prolate to triaxial fabrics (Figs 4b-d).

S2

Field observations

Inclined sheet S2 is 50 cm thick and displays a prominent ‘ramp-flat’ morphology (Fig. 5a); S2 is observed to transgress the interbedded limestones and shales (160/09° SW) of the Blue Lias Formation at 048/44° NW towards its western extent (NM 49271 62680; 56°41’18”N 6°05’46”W), before abruptly becoming strata-concordant (154/10° SW) (Figs 5a and b). Extrapolation to the east of the ‘flat’ S2 section highlighted in Figure 5b suggests that a second outcrop of strata-concordant

(140/16° SW) S2 is preserved at NM 49278 62664 (i.e. 56°41'18"N 6°05'46"W) (Fig. 5a). Both outcrops are mineralogically identical, consisting of a medium-grained (<1.5 mm) diabase that contains coarse (up to 3 mm) pyroxene and sulfide blebs. No chilled margins were observed and there is no apparent grainsize variation at hand specimen scale across the inclined sheet.

Magnetic fabrics and susceptibilities

Two sites were selected for analysis within S2; four profiles (i.e. S2a-d) were collected from the western outcrop and three profiles (i.e. S2e-g) from the eastern outcrop (Figs 5 and 6). The two sites display a distinct difference in K_{mean}, with S2a-d ranging from 4.13×10^{-2} SI to 5.40×10^{-2} SI and S2e-g ranging from 1.62×10^{-2} SI to 1.93×10^{-2} SI (Table 1). No intra-site variation is observed within the P_j values (1.11–1.17) and the T data indicate that, with the exception of S2a (T = 0.358), all profiles contain magnetic fabrics that are near triaxial to prolate (T = -0.181 to -0.819). The sub-horizontal magnetic lineations, which trend NW-SE, also remain remarkably consistent regardless of sheet orientation and are thus considered reliable (Figs 5 and 6). Typically, the magnetic foliations strike NW-SE, parallel to the magnetic lineation trend, apart from S2a which is oriented 049/17° NW (plunge azimuth and plunge). Only the S2a and S2d magnetic foliations are located close to the plane of the intrusion (Figs 5 and 6). However, whilst the majority of the magnetic foliations are thereby oriented out of the intrusion plane, it is important to note that the extension of the K_2 and K_3 girdles implies that the magnetic foliations corresponding to S2b, S2c, and S2e-g may not be reliable (Figs 5 and 6). The principal susceptibility axes of S2d are sub-parallel to those measured by Magee et al. (2012a) for a sample (i.e. CS166) from approximately the same position (Fig. 5C).

S3

Field observations

The only dike analyzed in this study (i.e. S3; 56°41’18”N 6°05’48”W) has a diabase composition and is oriented 152/90° (Fig. 3a). Sample S3 is planar and cross-cuts the Blue Lias Formation and earlier Paleogene inclined sheet intrusions (Fig. 3a). Cross-cutting relationships indicate that dike intrusion post-dated tilting of the Blue Lias Formation and emplacement of the inclined sheets (Fig. 3a), which occurred in response to the inflation and growth of the Ardnamurchan Central Complex; i.e. the contemporaneous local stress field was characterized by a radially inclined σ_1 and a circumferential σ_3 (Magee et al. 2012a). The relatively young age of S3 and its vertical nature (i.e. suggestive of a horizontal σ_3), imply that dike emplacement occurred after the cessation of magmatic activity on Ardnamurchan. It is likely that S3 represents a ‘so-called’ regional dike given that its orientation (152/90°) is parallel to that of the regional dike swarm (160-340°) exposed locally (Speight et al. 1982). Dike thickness varies along strike from ~1.5–3 m. The dike consists of fine (≤1 mm) plagioclase, clinopyroxene, and titanomagnetite with no phenocryst phases present. Grainsize does not appear to vary across the intrusion at hand specimen scale.

Magnetic fabrics and susceptibilities

Two separate sites 60 m along strike were analyzed within S3 (Fig. 3a); at each site, western and eastern contact-parallel profiles and a sheet-normal traverse were sampled (Fig. 7). The K_{mean} values of S3a-c (4.91×10^{-2} SI, 5.21×10^{-2} SI and 4.92×10^{-2} SI, respectively) are slightly lower compared to S3d-f (5.21×10^{-2}, 5.22×10^{-2} and 5.90×10^{-2}, respectively), but within all six profiles there is a degree of internal variability that is independent of P_j (Fig. 7; Table 1). For all six profiles, the magnetic lineation and the magnetic foliation are located within or close to the plane of intrusion (Fig. 7). The magnetic lineation is typically sub-vertical, with plunges ranging from 74–88°, although the S3a K_1 is oriented at 144/26° (plunge azimuth and plunge) (Fig. 7; Table 1). Figure 7 highlights that some subtle variations between the magnetic foliation and intrusion plane occur across the dike. The magnetic foliations in S3a-c all dip at ~86° towards the NE but strike rotates from 146° along the western margin to 164° at the eastern margin. The strikes of the S3d-f magnetic foliations display a similar rotation from 138° (western margin) to 151° (eastern margin) across the dike (Fig. 7a). However, it is important to note that the magnetic foliations from the margin samples dip in opposite directions; S3d dips 81° to the SW whilst S3f dip north-eastwards at 84° (Fig. 7a). Within both S3b and S5e, the two sheet-normal traverses, the magnetic fabric orientations remain remarkably consistent (Fig. 7a).

For the three S3a-c samples, P_j is relatively consistent (1.065, 1.068 and 1.073, respectively) whist T values range from 0.49 to 0.79 (oblate). Although the P_j values of S3d-f are similarly consistent (1.028, 1.030 and 1.039, respectively), albeit lower, the shape of the magnetic fabric is triaxial (T = 0.05, 0.26 and 0.09, respectively). Within S3e it is apparent that the most oblate fabrics commonly occur along the dike margins whilst the triaxial fabrics occur primarily within a thin (~25 cm wide) zone offset to the SW of the dike center by ~25 cm (Fig. 7b). These triaxial fabrics also spatially correspond to a zone of decreased P_j (Fig. 7b). A similar internal variation is not observed in S3b, where P_j (1.068–1.077) and T (0.49–0.62) are both tightly constrained and uniform (Fig. 7a).

S4

Field observations

Along its ~100 m length (centered on 56°41’33”N 6°04’44”W), S4 displays a highly variable dip, of 7–58°, compared to the consistent orientation (~046/05° W) of the Pabay Shale Formation host rock (Figs 8a and b). Sheet thickness is similarly variable and ranges from 1 m up to 5 m (at S4e and S4f) (Figs 8a and b). In two locations, S4 is cross-cut by dikes trending 151–331° and 156–336° (Figs 8a and b). The intrusion is aphyric with grainsizes <1.5 mm; with the exception of a thin <1 cm chilled margin, no grainsize variation is observed across the inclined sheet at hand specimen scale.

Magnetic fabrics and susceptibilities

Six sample suites were collected from S4 (Fig. 8): (i) the S4a-c profiles sample the base, middle, and top of the 2 m thick inclined sheet (038/07° W) where a small (~10 cm high) intrusive step, bearing 163–343°, occurs; (ii) S4d samples the moderate-to-steeply dipping portion (035/58° W) of S4 to the north of the S4a-c site and approximately corresponds to the CSJ1 AMS sample position of Magee et al. (2012); and (iii) S4e and S4f were taken from the southern extent of the inclined sheet (020/46° W), at the low tide mark, where sheet thickness increases to ~5 m. The range of K_{mean} values for all samples is relatively limited, ranging from 2.57×10^{-2} SI to 4.15×10^{-2} SI (Table 1). Overall, the magnetic fabrics show a relatively weak anisotropy (P_j = 1.015–1.031) and are near triaxial to prolate (T = -0.109 to -0.736) (Table 1). Although the magnetic fabric orientation is variable, K_1 typically plunges (33–59°) to the NW and is within or close to the plane of the intrusion (Fig. 8c). These magnetic lineations are either parallel or oblique (by up to 50°) to the inclined sheet dip direction (Fig. 8c). The one exception to this is S4a where K_1 is orthogonal to the intrusion plane (Fig. 8c). Magnetic foliations range in dip from 49–87° and display variable strike orientations (Fig. 8c). Three profiles reveal magnetic foliation strikes that are parallel to the inclined sheet dip direction (i.e. S4a, b and e), whilst two are oblique (i.e. S4d and f) and one is parallel (i.e. S4c) to the sheet strike (Fig. 8c). There are little to no systematic variations in the magnetic fabrics across the sheet width or along strike, regardless of sheet orientation (Fig. 8c). For example, S4d yields a similar magnetic fabric to the CSJ1 sample measured by Magee et al. (2012) from the same locality (Fig. 8c).

S5

Field observations

The S5 fine-grained (≤1 mm), diabase inclined sheet (NM46527 62255; 56°41’10”N 6°08’02”W) is oriented at 042/22° NW and intrudes a massive diabase unit, the overall geometry of which cannot be distinguished in the field due to a paucity of exposure (Figs 2 and 9). Along strike, the thickness of the inclined sheet varies from <1 m up to 3 m (e.g., Fig. 9).

Magnetic fabrics and susceptibilities

Within S5, three profiles were analyzed that correspond to the top (S5a), middle (S5b), and base (S5c) of the inclined sheet; a vertical traverse was sampled (S5d) (Fig. 9). K_{mean} values for all samples range from 3.33×10^{-2} SI to 4.65×10^{-2} SI (Table 1). With the exception of the basal profile (S5c), which has a P_j value of 1.009, the Pj range is relatively restricted to 1.022–1.029 (Table 1). Overall, the T data suggest that the magnetic fabrics are generally triaxial, although there is a range from near prolate (i.e. S5b = -0.460) to near oblate (i.e. S5a = 0.316) (Table 1). Magnetic lineations all trend NW-SE, with plunges ranging from 2–27°, sub-parallel to the strikes of the magnetic foliations (Fig. 9; Table 1). This NW-SE trend is sub-parallel to the dip direction of the inclined sheet (Fig. 9). The spread of individual principal susceptibility axes in the vertical traverse (i.e. S5d) is likely due to poorly constrained magnetic fabrics in the base of the intrusion (cf. S5c) (Fig. 9).

S6

Field observations

The diabase inclined sheet S6 is fine-grained (≤1 mm), oriented at 096/30° N, and located along the Ormsaigbeg shore (56°41’09”N 6°08’03”W) (Fig. 2). It is emplaced into the Bearreraig Sandstone Formation (083/30° S) and thins eastwards along strike from 2 m to 1 m. A small intrusive step (~10–20 cm high), with a long axis bearing 158–338° (Fig. 10), is observed at the basal contact.

Magnetic fabrics and susceptibilities

Four sample suites were collected from S6, including transects along the base, middle, and top of the intrusion as well as a vertical traverse (i.e. S3a-d, respectively) (Fig. 10). K_{mean} ranges from 3.68×10^{-2} SI to 5.28×10^{-2} SI whilst P_j (1.026–1.043) and T (-0.049 to 0.038; triaxial) show little variation (Table 1). Similarly, the magnetic fabric orientations remain remarkably consistent regardless of sample location; K_1 is, on average, oriented at 350/18° (plunge azimuth and plunge) and the magnetic foliation (106/20° N average) is sub-parallel to the plane of intrusion but does display a consistently shallower dip (Fig. 10).

S7

Field observations

S7 is located to the east of Ben Hiant (at 56°42’22”N 5°59’50”W), has a medium-grained (~2–3 mm) diabase composition, consisting primarily of plagioclase, clinopyroxene and titanomagnetite. It is intruded into a series of vertically stacked, sub-horizontal olivine-basalt lavas (<1 mm grain-size) but no host rock contacts are exposed. Figure 11 reveals that S7 can be sub-divided into four outcrops (~30–50 m width), bounded by subtle topographic depressions, which individually display slight variations in thickness (~1.5–2 m) at regular intervals along strike. Each outcrop represents the southern extremity of an elongated ‘lobe-like’ ridge (~<5 m high), which extend northwards for up to ~200 m and have azimuths ranging from 116-296° in the NE to 161-341° in the SW (Figs 11a-c). From NE to SW, the four outcrops have approximate strikes and dips of 037/30° WNW, 058/30° NW, 080/30° N and 074/30° N (Fig. 11a). Towards the margins of each outcrop, grain-size decreases to ~1 mm and contains an increasing proportion of calcite-bearing amygdales (up to 8 mm diameter). Superimposed onto each ‘lobe’ are a series of sub-parallel troughs (~<0.5 m deep), which extend northwards from the outcrops for ~10 m (Fig. 11b) and spatially correspond to the zones of observed thinning (Fig. 11c). Beyond the northern limit of the lobes, a small monocline is developed within the lava flows (Figs 11a and b).

Magnetic fabrics and susceptibilities

Four sites within S7 were selected for high resolution AMS analysis (Fig. 11a); S7a was collected from the north-easternmost outcrop (NM 55401 64253), S7b-c are from the same outcrop (NM 55421 64327 and 55513 64422, respectively) and S7d corresponds the most south-western outcrop sampled (NM 55324 64217). The K_{mean} values for each site are 3.68×10^{-2} SI, 6.87×10^{-2} SI, $5.79 \times$

10^{-2} SI, and 3.64×10^{-2} SI, respectively (Table 1). Values for P_j and T range from 1.019–1.141 (weak to strong anisotropy) and -0.274–0.566 (prolate-triaxial to oblate), respectively (Table 1). The magnetic fabric for each site is relatively well constrained and reveals that K_1 is approximately orthogonal to the plane of intrusion (Fig. 11d); the magnetic lineation values (plunge azimuth and plunge) are 144/44°, 171/58°, 107/67° and 141/32° for S7a-d. These magnetic lineations are sub-parallel to the elongation direction of their respective lobe-like ridge (Fig. 11D). Similarly, the magnetic foliation is oriented out of the plane of intrusion and either dips moderately to the south (102/55° S, S7a; 094/59° S, S7b) or steeply to the east (157/72° S, S7c; 144/85° S, S7d) (Fig. 11d).

Rock magnetic experiments

Rock magnetic experiments provide important insights into the magnetic mineralogy of a rock, particularly for fine-grained rocks (e.g., those analyzed here) where traditional petrography is difficult. Samples S3b, S3f, S4c, and S5b were selected for low-field susceptibility versus high-temperature experiments because: (i) the S3 samples represent apparently 'normal' magnetic fabrics and allow internal variations in magnetic mineralogy to be assessed (Fig. 7); (ii) the S4c magnetic fabric is oblique to the intrusion and could therefore be interpreted as an imbricated fabric or an 'intermediate' or 'inverse' fabric (Fig. 8c); and (iii) S5b appears to be an 'inverse' fabric (i.e. the magnetic lineation and foliation are approximately orthogonal to the intrusion plane; Fig. 9). The four samples generally show an increase in susceptibility on heating until a sharp downward deflection (i.e. a Hopkinson Peak) occurs at 559°C (Figs 12a-d). Convex-upward 'bumps' are superimposed onto this heating trend for S4c and S5b (Figs 12c and d). For S4c, the shallow 'bump' spans a temperature range of 131–350°C and attains a maximum susceptibility of 274 SI at 287°C (Fig. 12c). The prominent 'bump' observed in the S5b heating curve spans 104–393°C and attains a maximum susceptibility of 823 SI at 289°C (Fig. 12d). Samples selected for hysteresis analysis apparently represent either 'normal' magnetic fabrics (S1a, S3a, S3f, and S6b) or possible 'inverse' fabrics (i.e. S4a and S4c) (Figs 4, 7, 8, and 10). Hysteresis loops for all samples show steep acquisition reaching saturation by 0.300 T and yielding moderately narrow-waisted loops consistent with a pseudo-single domain grain size. Figure 12e shows that the samples chosen for hysteresis analysis all plot within the pseudo-single domain field of a standard Day plot.

Interpretation

Magnetic fabric origin

Estimating primary magma flow patterns within ancient sheet intrusions is integral to understanding the transport and accommodation of magma within active sub-volcanic systems. Although numerous studies have successfully demonstrated the correlation between primary magma flow and magnetic fabrics (e.g., Callot et al. 2001; Aubourg et al. 2002; Liss et al. 2002; Horsman et al. 2005; Morgan et al. 2008), the interpretation of AMS measurements as reliable flow indicators remains controversial. Before AMS data can be used to interpret magma flow patterns, it is essential to define the magnetic mineralogy (i.e. what carries the magnetic signature of the rocks) and the origin of the magnetic fabric (e.g., has it been modified by post-emplacement tectonic activity?).

Magnetic mineralogy

From petrographic analyses and rock magnetic experiments, Magee et al. (2012a) and Magee et al. (2013b) suggested that the magnetic signature of inclined sheets in Ardnamurchan is dominated by a low-Ti titanomagnetite phase. The following observations support the dominance of low-Ti titanomagnetite on the magnetic signature of the sheets studied here: (i) relatively high K_{mean} values of >1.62 × 10^{-2} SI (Tarling and Hrouda 1993); and (ii) general increases in susceptibility on heating up to 559°C (i.e. the Curie Point of each sample) before a rapid decrease upon further heating (Fig. 12), which based on the equations of Akimoto (1962) is consistent with a Ti content of ~0.039 (see Dunlop and Özdemir 2001). The 'bumps' observed along the heating curves for S4c and S5b in the low susceptibility versus temperature experiments are typically interpreted to result from the homogenization of two Fe-Ti oxide phases, and likely suggest that titanomaghemite may contribute to the magnetic signature of some samples; although monoclinic pyrrhotite also has a Curie point (320ºC) in this temperature range (see Dunlop and Özdemir 2001). Magee et al. (2013b) also highlighted that some inclined sheets may contain populations of single-domain magnetite, which could potentially alter the orientation of the magnetic fabric by switching the principal susceptibility axes to form intermediate or inverse magnetic fabrics (cf. Rochette et al. 1999; Ferré 2002). Figure 12e indicates that all of the samples analyzed are dominated by pseudo-single domain titanomagnetite populations, implying that, at least for S1a, S3a, S3f, S4a, S4c, and S6c, the magnetic fabrics can be classified as 'normal'.

Magnetic fabric origin

Magee et al. (2012a) and Magee et al. (2013b) demonstrated that the shape and distribution of titanomagnetite populations within the Ardnamurchan inclined sheets was controlled by the primary silicate framework. This implies that the magnetic fabrics correlate with the petrofabric of the silicate grains. If the mineral fabrics were generated by magma flow, it is typically expected that K_1 and the magnetic foliation will be located within or close to the plane of intrusion (i.e. the magnetic fabrics are 'normal') and that the magnetic lineation may correspond to the magma flow axis (cf. Knight and Walker 1988; Rochette et al. 1999; Ferré 2002). Magee et al. (2012a) argued that magma flow patterns are discernible in inclined sheets on Ardnamurchan by combining the orientation of identified normal magnetic fabrics, particularly magnetic lineations, with measurements of the long axes of visible flow indicators such as intrusive steps, broken bridges, and magma lobe axes. Where similar intrusive steps are observed in the inclined sheets analyzed here (i.e. S4a-c, S6, and S7), the orientation of the magnetic lineation is sub-parallel to that of the step long axes (Figs 8 and 10). This suggests that the magnetic fabrics can be correlated with magma flow.

However, several alternative options need to be explored when interpreting magnetic fabrics as related to magma flow. For example, many of the inclined sheet intrusions analyzed here were emplaced at relatively shallow levels but apparently lack chilled margins (see also Magee et al. 2012a and references therein), implying that either the: (1) temperature of the host rock during the emplacement of the inclined sheet swarm was elevated by the local magmatic activity (Day, 1989), inhibiting chilled margin formation; or (2) magma flow within the individual sheets was protracted and instigated melt-back of any chilled margin originally present (e.g., Huppert and Sparks, 1989). It is therefore difficult to discern whether magnetic fabrics correspond to initial propagation or magma flow within a more mature system (e.g., Liss et al. 2002; Philpotts and Philpotts, 1997). Furthermore, it is important to note that measured magnetic lineations and/or magnetic foliations do not always lie close to the plane of the intrusion (e.g., Figs 3-6, 8, 9, and 11). Such disparities between the orientation of the intrusion and the magnetic fabrics are commonly interpreted as intermediate or inverse fabrics produced by the presence of a single domain titanomagnetite population within a sample (e.g., Potter and Stephenson 1988; Rochette and Fillion 1988; Borradaile and Puumala 1989). Importantly, hysteresis experiments demonstrate that S4a and S4c, which record magnetic fabrics that are strongly oblique to the intrusion plane, do not contain single domain titanomagnetite populations (Fig. 12e). This implies that apparently intermediate and inverse fabrics cannot necessarily be attributed to complexities in the magnetic mineralogy. Instead, these anomalous magnetic fabrics may result from cyclic crystal behavior during magma flow and/or post-emplacement processes (Cañón-Tapia and Herrero-Bervera 2009). Because Ardnamurchan remained relatively tectonically inactive after the formation of the central complex (Emeleus and Bell 2005), any post-emplacement superimposition of magnetic fabrics would likely have resulted from either: (i) convection within individual inclined sheets; (ii) inflation or deflation of later major intrusions (e.g., the Gabbro lopolith); or (iii) roof subsidence and intrusion closure, instigated by the waning of magma pressure, within the inclined sheets during the final stages of emplacement.

We consider it unlikely that convection modified most of the magnetic fabrics measured because the majority of sampled sites occur where the inclined sheets have thicknesses <3 m (e.g., Figs 4, 5, 8, 9, and 11); i.e. heat loss is expected to be relatively rapid, inhibiting convection. If convection did occur in any of the sheet intrusions studied, it may be expected that the thickest intrusion (i.e. the S4e-f sample site where inclined sheet thickness increases to 5 m) would record the strongest evidence of convection within the magnetic fabrics. We suggest that if convection were to have occurred in the thicker portions of S4, the associated magnetic fabrics should differ to those measured in thinner sections of the intrusion. However, AMS results for S4 all display magnetic lineations that approximately trend NW-SE, parallel to the long axis of an intrusive step (i.e. a visible magma flow indicator) observed near S4a-c (Fig. 8). These observations suggest that convection did not modify the magma flow related petrofabrics.

Deformation of the inclined sheets, induced by either major intrusion growth or roof subsidence, would likely effect entire inclined sheets. We assume that at any one sample site, application of a post-emplacement strain capable of modifying petrofabrics will act to homogenize the magnetic fabric orientation, although irregularities in sheet geometry at different sites may promote variations in post-emplacement fabrics. Given the sub-circular nature of the exposed major intrusions and the arcuate strike of the inclined sheets (Fig. 2), we would expect that any non-magma flow, compaction related fabrics should be: (i) oblate, with magnetic foliations that parallel intrusion contacts; and (ii) typically consistent along the strike of individual inclined sheets. However, the broad range of magnetic fabric orientations measured here and in the study of Magee et al. (2012a), some of which do not lie close to the plane of intrusion, suggest that the magnetic fabrics were not formed by post-emplacement tectono-magmatic events. Similarly, quantitative textural analysis of several inclined sheets within the Ardnamurchan Central Complex suggest that they have undergone minimal textural equilibration following emplacement (Magee et al. 2013a). Given the lack of evidence for post-emplacement fabric modification, as well as the observed parallelism between magnetic lineations and field flow indicators (e.g., Figs 8 and 10) (Magee et al.

2012a), we suggest that the magnetic fabrics dominantly record primary magma flow. Through the integration of magnetic fabric analyses and structural field observations, the following sub-sections outline the interpretation of the emplacement of the individual sheet intrusions studied.

S1

Regardless of AMS sample location the magnetic fabrics within S1 are weakly to strongly prolate (-0.169 to -0.839) and K_1 gently plunges (~21°) NW-SE (~134–314°) sub-parallel to sheet strike (Fig. 4b). If it is assumed that the magnetic lineation reflects the axis of primary magma flow, the measured K_1 would imply magma within S1 either flowed towards the NW or SE, along sheet strike. However, the magnetic foliations display variable orientations, although the majority strike sub-parallel to S1, and at S1a-d define an imbrication suggestive of a SW directed magma flow pattern. In contrast, the magnetic foliations derived from S5e-h do not display a clear imbrication pattern but rather describe a progressive rotation from south-easterly inclined magnetic foliations at the sheet base to moderately inclined NE-dipping foliations near the top.

There are a number of interpretations that may be invoked to explain these observed complexities in the magnetic fabrics. Although S1a does not contain a single domain titanomagnetite population, we cannot rule out the possibility that magnetic fabrics recorded for other profiles within S1 are intermediate or inverse (cf. Rochette et al. 1999; Ferré 2002). Two alternative mechanisms for generating different magnetic foliations via variations in primary magma flow dynamics may also be considered. First, several studies have highlighted that different magnetic fabrics may be recorded at intrusion margins, particularly those that are chilled, compared to within the core of the sheet (e.g., Liss et al. 2002; Philpotts and Philpotts 2007). This is because chilled margins are likely to record sheet initial propagation fabrics and high simple shear gradients, whilst intrusion cores could preserve either regional magma flow patterns, different magma pulses, or convection in a relatively mature conduit (Liss et al. 2002). We consider it unlikely that the magnetic fabrics measured relate to differences in the style of fabrics recorded at the margins and the core because the chilled margin at S1 is <1 cm thick and therefore below our resolution of sampling (i.e. AMS cores are 2.5 cm in diameter). An alternative explanation concerns the common assumption that magma flow remains uniform along the strike of the magma flow direction (e.g., Callot et al. 2001; Correa-Gomes et al. 2001; Féménias et al. 2004). Magee et al. (2013b) suggested that sheet intrusions may be internally compartmentalized, implying that magma flow patterns could vary laterally within individual inclined sheets. Such compartmentalization could be associated with the observation that sheet intrusions are typically emplaced initially as a series of thin, discrete segments, which only coalesce upon continued magma input (see Schofield et al. 2012b and references therein). Any minor variations in the rheology and/or flow temperature of these discrete segments could promote subtle differences in their magma flow dynamics, which may be maintained upon coalescence and effectively compartmentalize the sheet intrusion (Magee et al. 2013a). In particular, lateral variations in magma flow dynamics would likely produce zones of relatively high velocity gradients that are orthogonal to intrusion contacts. Figure 13 is a schematic diagram, based on the magnetic fabric data from S1, which illustrates a potential interpretation of the spatial variations in magnetic fabrics, in light of the discussion above.

S2

Many sheet intrusions observed in field- (e.g., S2) and seismic reflection-data have a ‘ramp-flat’ morphology; i.e. whereby an inclined sheet transgresses stratigraphy before eventually becoming strata-concordant as a bedding plane or weak lithology is exploited (e.g., Thomson and Schofield 2008; Magee et al. 2012a; Muirhead et al. 2012; Magee et al. 2014). Commonly, the inclined sheets are fed via sills, although this can be difficult to corroborate in the field. It is important to note that these ramp-flat structures are not related to intrusive steps and that magma flow is expected to be (close to) parallel to the dip direction of the inclined sheet portion. For S2, this sheet geometry would imply that magma flowed from the NW to the SE (i.e. dip-parallel overall), consistent with the trend of the measured magnetic lineations (Figs 5 and 6).

S3

A magnetic analysis of a diabase dike was conducted to provide a comparison with the inclined sheets examined. Magnetic lineations and foliations are all located within the plane of intrusion with K_1 primarily being sub-vertical (Fig. 7). The exception to this is S3a, where K_1 plunges 144/26° (Fig. 7a), but this value may not be reliable due to the strongly oblate nature of the magnetic fabric (T = 0.79) and the spread of observed specimen data. Subtle variations in the magnetic foliation, including S3a, define an imbrication that opens down-dip (Fig. 7). Overall, the magnetic fabrics are consistent with an upwards-directed magma flow (i.e. dip-parallel), slightly offset from vertical towards the SE. A magma flow origin of the magnetic fabric could be further supported if the decrease in the oblateness of the magnetic fabrics towards the core of the S3e traverse is assumed to relate to the increased friction between magma and host rock towards intrusion contacts, which generates a high velocity gradient and oblate fabrics (Féménias et al. 2004). Alternatively, the margins of S3 may preserve fabrics from an initial period of higher flow strength compared to the core, which could host magnetic fabrics related to a later phase of decreasing magma flow. Similar fabric variations may not be observed in S3b because: (i) the sample spacing could be too coarse; or (ii) the increased width of the intrusion (i.e. 3 m relative to 1.5 m at S3e) may not be conducive to the preservation of the full velocity profile. It is, however, difficult to determine the process driving the recorded magma flow; e.g., is the magnetic fabric related to emplacement or subsequent convection.

S4

The along strike variation in the dip of S4 (~7–58°) can be considered a primary emplacement feature because there is no associated change in bedding orientation (Fig. 8), which would be indicative of subsequent tilting. Sheet thickness is also observed to range from ~2–5 m. Despite this variation in sheet geometry, encompassed by the three sites targeted for AMS, there is little systematic change in the magnetic fabric (orientation, shape or strength of anisotropy) (Fig. 8). For example, with the exception of S4a, which displays a steep magnetic lineation and a weakly defined magnetic foliation, K_1 axes plunge NW at 33–59° and parallel the long axis of an intrusive step (Fig. 8c). Magnetic foliations are consistently oriented at a high angle to the sheet dip and also occasionally to the intrusion strike (Fig. 8c). Because K_1 remains in the same approximate position throughout the samples, the orientation of the magnetic foliation is controlled by the K_2 axis, which appears to switch with K_3 (Fig. 8c). These deviations in the magnetic foliation orientation may relate to either: (i) complex and localized variations in magma flow dynamics within a single intrusion (e.g., Fig. 13); (ii) the sampling of different magma pulses with differing magma flow patterns (Liss et al. 2002); or (iii) the occurrence of a sufficient proportion of single-domain magnetite, in samples other than S4a and S4c (Fig. 12e), to produce mixed fabrics, as discussed above (cf. Rochette et al. 1999; Ferré 2002). Although adequate information to distinguish between these hypotheses is lacking, the parallelism between the magnetic lineations, sheet dip direction and the orientation of an intrusive step long axis implies that magma flow can still be elucidated (at least locally in the sheet) and was dip-parallel. The AMS sample analyzed by Magee et al. (2012a) from the northern exposure limit of S4 (i.e. their CSJ1) is parallel to the fabric described from within S4d (Fig. 5c).

S5

The parallelism between the magnetic lineations and the dip direction of S5 suggest that emplacement may have occurred in a north-westward or south-eastward direction (Fig. 9). Unfortunately there is not enough information to determine if the magnetic foliations, which are moderately to steeply dipping and strike parallel to the intrusion dip direction, reflect variations in primary magma flow patterns or the development of intermediate and/or inverse magnetic fabrics.

S6

Throughout S6, the AMS data are remarkably homogeneous (Fig. 10). The triaxial fabric ellipsoids consistently display a K_1 axis oriented sub-parallel to the dip and dip direction of the inclined sheet (083/30° N strike and dip) as well as the orientation of a minor intrusive step (~158-338° bearing) (Fig. 10). Although S6 thins to the east of the sample site from 2 m to 1 m, a morphological feature often inferred as a proxy for the magma flow direction (i.e. sheet intrusions are expected to thin towards their propagating tip; e.g., Hansen et al. 2011), the magnetic fabrics and intrusive step suggest that the magma flow axis was dip-parallel (i.e. oriented NNW-SSE). Thus, intrusion thinning may here be related to increasing proximity towards the lateral tip of the intrusion.

S7

The four discrete outcrops comprising S7 are considered to represent a single intrusion because they are petrologically similar and display a consistent ~NE-SW strike and northwards inclination (~30°) (Fig. 11). Apparent lobe-like elongations developed to the NW of the individual outcrops, distinguished by subtle topographic changes and the presence of small diabase outcrops, and the intervening topographic troughs may reflect either post-emplacement erosion or are a primary morphological feature (Figs 11a and b). Chilled margins and increasing amygdale abundance towards the upper, lower and lateral contacts of each lobe-like segment support an emplacement-related origin to the outcrop pattern observed. Similar magma lobe geometries have been described from the transgressive, inclined rims of saucer-shaped sills observed both in the field (e.g., Polteau et al. 2008; Schofield et al. 2010) and in seismic reflection data (Thomson and Hutton 2004; e.g., Schofield et al. 2012a; Magee et al. 2013b). These studies have shown that magma lobes form through the coalescence of magma fingers; i.e. thin, elongated magma conduits with an elliptical cross-section that may be emplaced in a non-brittle fashion in response to intrusion-induced host rock fluidization (Schofield et al. 2012b). Internal variations in the thickness of the S7 segments are consistent with the growth of magma lobes through the amalgamation of inflating magma fingers. Schofield et al. (2012b) describe similar magma fingers in a diabase inclined sheet intrusion located

~300 m to the west of S7 and emplaced into a succession of Neoproterozoic Moine Supergroup metasedimentary rocks and Paleogene volcaniclastics and olivine-basalt lavas. The magma fingers are only observed within the poorly consolidated lavas and volcaniclastics, where intrusion-induced collapse of the host rock pore space accommodated the magma volume and promoted non-brittle emplacement (Schofield et al. 2012b). It seems plausible that similar processes may have controlled the intrusion of S7 into the olivine-basalt lavas. Importantly, long axes of magma lobes and fingers can be used as a proxy for the primary magma flow axis (Schofield et al. 2012b). The north-westward elongation of the magma lobes and fingers documented here therefore implies a dip-parallel, NW-SE oriented, magma flow axis (Fig. 11a). Given the radial disposition of the four S7 outcrops, i.e. their long axes rotate from 166-296° in the NE to 161-341° in the SW, it is suggested that magma was fed from the NW (Fig. 11a). Figure 11 highlights that the projected source position corresponds to the location of a NE-SW trending monocline in the olivine-basalt lavas. This monocline might be the manifestation of roof uplift and forced folding above a tabular intrusion from which the S7 magma lobes emanated. This model and the S7 field observations are reminiscent of magma lobe structures described from the inclined limbs of saucer-shaped sills, where transgression was promoted by fracturing or fluidization of the host rock at points of maximum flexure on the fold (Thomson and Schofield 2008; Schofield et al. 2010).

Considering the possibility that S7 represents the southern inclined limb of a saucer-shaped sill centered to the north, it is apparent that the visible magma flow indicators (i.e. magma lobe and finger long axes) are not corroborated by the AMS results presented here (Fig. 11) or those of Magee et al. (2012a) (i.e. their samples CS111-115). The model proposed requires an upwards and outwards magma flow pattern, implying K_1 should plunge to the NW and be located within the plane of intrusion. Regardless of the sample position, Figure 11d reveals that K_1 is instead located near the normal to the intrusion plane. Similarly, magnetic foliations strike sub-parallel to the sheet intrusion dip direction and are nearly orthogonal to the intrusion plane (Fig. 11d). These measurements imply that the magnetic fabrics do not correspond to the primary magma flow pattern and may instead reflect an inverse or unstable magnetic fabric (cf. Rochette et al. 1999; Ferré 2002; Cañón-Tapia and Herrero-Bervera 2009).

Discussion

Our results show that integrated analyses combining AMS, rock magnetic experiments, and structural field observations allow inferences about magma flow patterns to be made. An important observation emanating from this study is that localized internal variations in the magnetic fabrics of inclined sheet intrusions may result from perturbations in the primary magma flow and are strongly controlled by sheet geometry. In particular, thinner sheet intrusions appear to display more uniform magnetic fabrics relative to thicker intrusions. This may be because: (i) chilled margins, which record the initial sheet propagation (e.g., Liss et al. 2002; Philpotts and Philpotts 2007) form a greater bulk of thinner intrusions; (ii) particle rotation and cyclicity during magma flow may be inhibited (see Canon-Tapia and Chavez-Alvarez 2004); or (iii) thicker intrusions may be composed of multiple magma pulses, each of which may contain subtly different mineralogies or magma flow patterns, or allow convection. The emplacement of subsequent magma pulses may additionally superimpose inflation-related sub-fabrics onto earlier, sub-solidus intrusive phases.

It is also important to consider how magma flow patterns may vary along strike. Many sheet intrusions are not emplaced as long, continuous bodies but rather form through the coalescence of discrete magmatic segments (e.g., Fig. 13A) (see Schofield et al. 2012b and references therein). If these individual segments become isolated following coalescence, perhaps due to the presence of internal chills or rheological boundaries, continued magma flow will therefore be influenced by high velocity gradients not just at the major intrusion margins but also at the lateral contacts (e.g., Fig. 13A) (Magee et al. 2013a). Inherently, the imbrication of magnetic foliations may be more complex than previously considered. Such an internal compartmentalization of sheet intrusions may compromise lateral mixing of magma or crystal populations (Magee et al. 2013a). To summarize, our results show that information pertaining to primary magma flow and inclined sheet emplacement can be elucidated given a thorough consideration of fabric relationships, magnetic mineralogy and field observations.

Ardnamurchan inclined sheet emplacement

The Ardnamurchan and Mull central complexes host the archetypal examples of cone sheet intrusions. Cone sheets have a (sub-)concentric strike and dip inwards towards a central source (Bailey 1924; Richey and Thomas 1930; Anderson 1936; Phillips 1974; Schirnick et al. 1999), from which the initial fracture and infilling magma is expected to propagate upwards and outwards (i.e. K_1 should be dip-parallel) (Herrero-Bervera et al. 2001; Geshi 2005; Palmer et al. 2007; Magee et al. 2012a). With the exception of S3, which likely represents a regional dike, the inclined sheets treated here have all previously been attributed to the cone sheet swarm on Ardnamurchan (Richey and Thomas 1930; Emeleus 2009; Burchardt et al. 2013).

Our results indicate that the inclined sheets studied across the southern portion of Ardnamurchan, excluding the S3 regional dike, are predominantly characterized by dip-parallel, NW-SE magma flow axes (i.e. S2, S4-S7; Fig. 14). The exception to this trend is S1, in which magma either flowed towards the SW (i.e. dip-parallel) or NW-SE (i.e. strike-parallel) depending on whether magnetic foliation imbrication or magnetic lineation trends, respectively, are used to define the magma flow pattern. These observations generally support the findings of Magee et al. (2012a), who noted that NW-SE oriented magnetic lineations dominated the Ardnamurchan inclined sheets (Fig. 14). From the 69 inclined sheets that Magee et al. (2012a) regarded as hosting reliable AMS fabric measurements, dip-parallel magma flow axes were only interpreted for 12 inclined sheets with the other 57 displaying strike-parallel magma flow patterns. These latter strike-parallel magnetic lineations were considered to reflect lateral magma flow along the inclined sheets, sourced from a reservoir external to the Ardnamurchan Central Complex; dip-parallel magma flow patterns were inferred to be fed from a central source beneath Ardnamurchan (Magee et al. 2012a). Within this study, magma flow directions could only be inferred from S2 and S7, with both suggestive of a source to the NW of the sampled exposures. Of these two inclined sheets, only the magma flow direction data for S2 is consistent with being fed from a central source within the Ardnamurchan Central Complex (Richey and Thomas 1930; Burchardt et al. 2013). The S7 intrusion appears to form part of a saucer-shaped sill, the source of which remains unknown.

Although the scope of this high-resolution magnetic fabric study is insufficient to determine whether the majority of inclined sheets were fed from a central source within the Ardnamurchan Central Complex (Burchardt et al. 2013) or an external reservoir (e.g., the Mull Central Complex; Magee et al. 2012a), it is worth highlighting: (i) that little, if any, post-emplacement modification of the magnetic fabrics has occurred; (ii) consistent NW-SE trending magnetic lineations and variable magnetic foliation orientations imply that the AMS fabrics likely correlate to primary magma flow; and (iii) inferred magma flow axes may be dip- or strike-parallel to the inclined sheet, indicative of both up-dip and lateral magma flow patterns, respectively. Burchardt et al. (2013) argued that lateral magma flow patterns inferred from inclined sheet AMS data (e.g., Magee et al. 2012a; this study) could be produced via the vertical translation of magma from a central source if a helical flow regime dominated inclined sheet emplacement. The only documented occurrence of helical flow concerns a composite, cylindrical pluton and is attributed to magma mixing (Trubač et al. 2009). However, for the Ardnamurchan inclined sheets, such a magma flow pattern requires that the sheets are fully concentric along strike; a geometry that is not consistent with geological maps or first-order field observations of the Ardnamurchan Central Complex, which reveal that the vast majority of inclined sheets (i.e. those not cross-cut by major intrusions) only extend along strike up to 1–2 kilometers but typically <100 m (Fig. 1) (Richey and Thomas 1930; Emeleus 2009). It is also important to note that the inclined sheets are represented diagrammatically on the geological map of Ardnamurchan (Richey and Thomas 1930 their statement on page 173); i.e. the mapped inclined sheet traces and dip values utilized by Burchardt et al. (2013) are local averages that have been extrapolated. Overall, our observations and interpretations here support the conclusion of Magee et al. (2012a) that inclined sheets on Ardnamurchan were sourced from magma reservoirs both central and external to the central complex. Petrological and geochemical (isotopic) analyses are required to further test this hypothesis.

Field observations reveal that the inclined sheets are geometrically complex and typically display significant variations in the strike and dip of individual intrusions (see also Richey and Thomas 1930; Kuenen 1937; Magee et al. 2012a; Magee et al. 2013a). These observations and the magnetic fabric analysis imply that the majority of sheet intrusions on Ardnamurchan may have a different down-dip extension to that previously envisaged, i.e. they do not converge upon a central source reservoir (e.g., S7) and that magma was sourced externally to the Ardnamurchan Central Complex (Magee et al. 2012a). These ideas highlight the danger in assuming that the dips of inwardly inclined sheets can be projected downward to infer magma chamber source locations (Richey and Thomas 1930; Burchardt and Gudmundsson 2009; Burchardt et al. 2013), although there are several examples where additional data (e.g., magma flow indicators) suggest that this approach may be applicable for constraining source characteristics (e.g., Geshi 2005). However, it is clear from field observations elsewhere (e.g., Burchardt 2008; Tibaldi and Pasquarè 2008; Muirhead et al. 2012; Schofield et al. 2012b) and seismic reflection data (e.g., Thomson and Hutton 2004; Planke et al. 2005; Magee et al. 2014) that the orientation of an intrusion at a specific level of exposure does not necessarily reflect that of the entire sheet, questioning the accuracy of models that are solely reliant on the planar projection of surficial strike and dip averages.

Conclusions

The analysis of ancient sheet intrusions exposed at the surface provides crucial insights into the emplacement mechanisms and magma flow patterns of active sub-volcanic plumbing systems. Here, we employ anisotropy of magnetic susceptibility (AMS) to examine magnetic fabrics within a suite of seven inclined sheet intrusions located on Ardnamurchan, NW Scotland. Despite a broad variation in the orientation of studied sheet intrusions, magnetic lineations predominantly trend NW-SE and have shallow to moderate plunges. Magnetic foliations within individual intrusions display more variation in their orientation and are not necessarily sub-parallel to the plane of intrusion. Through the integration of AMS, rock magnetic experiments and structural field observations, we demonstrate: (i) that the magnetic signature is dominated by low-Ti titanomagnetite populations, which commonly have a pseudo-single domain grainsize; (ii) the measured magnetic fabrics are complex and variable within individual intrusions; (iii) little post-emplacement modification of the magnetic fabrics has occurred; and (iv) that the magnetic fabrics likely reflect primary magma flow. By considering the magnetic fabric orientation and their location within each intrusion we show that inferred magma flow axes for at least five intrusions are typically dip-parallel and oriented NW-SE. One intrusion potentially displays evidence for strike-parallel magma flow directed towards the SW. Importantly, our results suggest that magma flow dynamics within individual intrusions can vary laterally, promoting the development of magma lobes which can effectively internally (petrologically) compartmentalize seemingly continuous sheets. This has important implications for understanding the channelization of magma within sheet intrusions, which can affect eruption locations and magma mixing trends.

Acknowledgements

We thank Trevor Potts for providing accommodation during the field campaign, which was funded by National Geographic Grants in aid of Research award #8106-06 to Petronis. The cored drill-holes produced over the course of this study were subsequently infilled under the guidance of Scottish National Heritage. We are grateful to three anonymous reviewers for their constructive comments. Tom Stone is thanked for his preliminary analysis on some of these samples for his MSci project.

Reference List

Abebe, B., Acocella, V., Korme, T. & Ayalew, D. 2007. Quaternary faulting and volcanism in the Main Ethiopian Rift. Journal of African Earth Sciences, **48**, 115-124.

Abelson, M., Baer, G. & Agnon, A. 2001. Evidence from gabbro of the Troodos ophiolite for lateral magma transport along a slow-spreading mid-ocean ridge. Nature, **409**, 72-75.

Akimoto, S. 1962. Magnetic properties of FeO-Fe2O3-TiO2 system as a basis of rock magnetism. Journal of the Physical Society of Japan, **17**, 706-&.

Anderson, E.M. 1936. Dynamics of formation of cone-sheets, ring-dykes, and cauldron subsidence. Proceedings of the Royal Society of Edinburgh, **56**, 29.

Anderson, E.M. 1937. Cone-sheets and ring-dykes: the dynamical explanation. Bulletin Volcanologique, **1**, 35-40.

Archanjo, C.J. & Launeau, P. 2004. Magma flow inferred from preferred orientations of plagioclase of the Rio Ceara-Mirim dyke swarm (NE Brazil) and its AMS significance. Geological Society, London, Special Publications, **238**, 285-298.

Aubourg, C., Giordano, G., Mattei, M. & Speranza, F. 2002. Magma flow in sub-aqueous rhyolitic dikes inferred from magnetic fabric analysis (Ponza Island, W. Italy). Physics and Chemistry of the Earth, Parts A/B/C, **27**, 1263-1272.

Aubourg, C., Tshoso, G., Le Gall, B., Bertrand, H., Tiercelin, J.J., Kampunzu, A.B., Dyment, J. & Modisi, M. 2008. Magma flow revealed by magnetic fabric in the Okavango giant dyke swarm, Karoo igneous province, northern Botswana. Journal of Volcanology and Geothermal Research, **170**, 247-261.

Bailey, E.B. 1924. Tertiary and Post-Tertiary Geology of Mull, Loch Aline, and Oban: A Description of Parts of Sheets 43, 44, 51, and 52 of the Geological Map. HM Stationery Office.

Borradaile, G. 1987. Anisotropy of magnetic susceptibility: rock composition versus strain. Tectonophysics, **138**, 327-329.

Borradaile, G. & Puumala, M. 1989. Synthetic magnetic fabrics in a plasticene medium. Tectonophysics, **164**, 73-78.

Borradaile, G.J. 1988. Magnetic susceptibility, petrofabrics and strain. Tectonophysics, **156**, 1-20.

Borradaile, G.J. & Henry, B. 1997. Tectonic applications of magnetic susceptibility and its anisotropy. Earth-Science Reviews, **42**, 49-93.

Bouchez, J.L. 1997. Granite is never isotropic: an introduction to AMS studies of granitic rocks. Springer.

Burchardt, S. 2008. New insights into the mechanics of sill emplacement provided by field observations of the Njardvik Sill, Northeast Iceland. Journal of Volcanology and Geothermal Research, **173**, 280-288.

Burchardt, S. & Gudmundsson, A. 2009. The infrastructure of Geitafell volcano, southeast Iceland. Studies in Volcanology: The Legacy of George Walker, Spec. Publ. of IAVCEI, **2**, 349-370.

Burchardt, S., Troll, V.R., Mathieu, L., Emeleus, H.C. & Donaldson, C.H. 2013. Ardnamurchan 3D cone-sheet architecture explained by a single elongate magma chamber. Scientific Reports, **3**, 2891.

Callot, J.-P. & Geoffroy, L. 2004. Magma flow in the East Greenland dyke swarm inferred from study of anisotropy of magnetic susceptibility: magmatic growth of a volcanic margin. Geophysical Journal International, **159**, 816-830.

Callot, J.-P., Geoffroy, L., Aubourg, C., Pozzi, J. & Mege, D. 2001. Magma flow directions of shallow dykes from the East Greenland volcanic margin inferred from magnetic fabric studies. Tectonophysics, **335**, 313-329.

Callot, J. & Guichet, X. 2003. Rock texture and magnetic lineation in dykes: a simple analytical model. Tectonophysics, **366**, 207-222.

Cañón-Tapia, E. 1996. Single-grain versus distribution anisotropy: a simple three-dimensional model. Physics of the Earth and Planetary Interiors, **94**, 149-158.

Cañón-Tapia, E. 2001. Factors affecting the relative importance of shape and distribution anisotropy in rocks: theory and experiments. Tectonophysics, **340**, 117-131.

Canon-Tapia, E. 2004. Anisotropy of magnetic susceptibility of lava flows and dykes: A historical account. Geological Society, London, Special Publications, **238**, 205-225.

Canon-Tapia, E. & Chavez-Alvarez, J. 2004. Theoretical aspects of particle movement in flowing magma: implications for the anisotropy of magnetic susceptibility of dykes. Geological Society, London, Special Publications, **238**, 227-249.

Cañón-Tapia, E. & Herrero-Bervera, E. 2009. Sampling strategies and the anisotropy of magnetic susceptibility of dykes. Tectonophysics, **466**, 3-17.

Cashman, K.V. & Sparks, R.S.J. 2013. How volcanoes work: A 25 year perspective. Geological Society of America Bulletin, **125**, 664-690.

Correa-Gomes, L., Souza Filho, C., Martins, C. & Oliveira, E. 2001. Development of symmetrical and asymmetrical fabrics in sheet-like igneous bodies: the role of magma flow and wall-rock displacements in theoretical and natural cases. Journal of Structural Geology, **23**, 1415-1428.

Cruden, A.R. & Launeau, P. 1994. Structure, magnetic fabric and emplacement of the Archean Lebel Stock, SW Abitibi greenstone belt. Journal of Structural Geology, **16**, 677-691.

Day, R., Fuller, M. & Schmidt, V. 1977. Hysteresis properties of titanomagnetites: grain-size and compositional dependence. Physics of the Earth and Planetary Interiors, **13**, 260-267.

Day, S.J. 1989. The geology of the Hypersthene Gabbro of Ardnamurchan Point and its implications for its evolution as an upper crustal basic magma chamber. Ph.D Thesis, **University of Durham**.

Dunlop, D.J. & Özdemir, Ö. 2001. Rock magnetism: fundamentals and frontiers. Cambridge University Press.

Ellwood, B.B. 1982. Estimates of flow direction for calc-alkaline welded tuffs and paleomagnetic data reliability from anisotropy of magnetic susceptibility measurements: central San Juan Mountains, southwest Colorado. Earth and Planetary Science Letters, **59**, 303-314.

Emeleus, C.H. 2009. Ardnamurchan Central Complex. Bedrock and Surperficial Deposits. . 1:25,000 Geology Series British Geological Survey. Keyworth, Nottingham (2009).

Emeleus, C.H. & Bell, B. 2005. The Palaeogene volcanic districts of Scotland. British Geological Survey.

Ernst, R.E. & Baragar, W.R.A. 1992. Evidence from magnetic fabric for the flow pattern of magma in the Mackenzie giant radiating dyke swarm. Nature, **356**, 511-513.

Féménias, O., Diot, H., Berza, T., Gauffriau, A. & Demaiffe, D. 2004. Asymmetrical to symmetrical magnetic fabric of dikes: Paleo-flow orientations and Paleo-stresses recorded on feeder-bodies from the Motru Dike Swarm (Romania). Journal of Structural Geology, **26**, 1401-1418.

Ferré, E.C. 2002. Theoretical models of intermediate and inverse AMS fabrics. Geophysical Research Letters, **29**, 31-31-31-34.

Gaffney, E.S., Damjanac, B. & Valentine, G.A. 2007. Localization of volcanic activity: 2. Effects of pre-existing structure. Earth and Planetary Science Letters, **263**, 323-338.

Gautneb, H. & Gudmundsson, A. 1992. Effect of local and regional stress fields on sheet emplacement in West Iceland. Journal of Volcanology and Geothermal Research, **51**, 17.

Gautneb, H., Gudmundsson, A. & Oskarsson, N. 1989. Structure, petrochemistry and evolution of a sheet swarm in an Icelandic central volcano. Geological Magazine, **126**, 14.

Geoffroy, L., Olivier, P. & Rochette, P. 1997. Structure of a hypovolcanic acid complex inferred from magnetic susceptibility anisotropy measurements: the Western Red Hills granites (Skye, Scotland, Thulean Igneous Province). Bulletin of Volcanology, **59**, 147-159.

Geshi, N. 2005. Structural development of dike swarms controlled by the change of magma supply rate: the cone sheets and parallel dike swarms of the Miocene Otoge igneous complex, Central Japan. Journal of Volcanology and Geothermal Research, **141**, 267-281.

Grégoire, V., de Saint Blanquat, M., Nédélec, A. & Bouchez, J.L. 1995. Shape anisotropy versus magnetic interactions of magnetite grains: experiments and application to AMS in granitic rocks. Geophysical Research Letters, **22**, 2765-2768.

Grégoire, V., Darrozes, J., Gaillot, P., Nédélec, A. & Launeau, P. 1998. Magnetite grain shape fabric and distribution anisotropy vs rock magnetic fabric: a three-dimensional case study. Journal of Structural Geology, **20**, 937-944.

Gudmundsson, A. 2002. Emplacement and arrest of sheets and dykes in central volcanoes. Journal of Volcanology and Geothermal Research, **116**, 279-298.

Gudmundsson, A. 2011. Deflection of dykes into sills at discontinuities and magma-chamber formation. Tectonophysics, **500**, 50-64.

Hansen, J., Jerram, D., McCaffrey, K. & Passey, S. 2011. Early Cenozoic saucer-shaped sills of the Faroe Islands: an example of intrusive styles in basaltic lava piles. Journal of the Geological Society, **168**, 159-178.

Hargraves, R., Johnson, D. & Chan, C. 1991. Distribution anisotropy: The cause of AMS in igneous rocks? Geophysical Research Letters, **18**, 2193-2196.

Herrero-Bervera, E., Walker, G., Canon-Tapia, E. & Garcia, M. 2001. Magnetic fabric and inferred flow direction of dikes, conesheets and sill swarms, Isle of Skye, Scotland. Journal of Volcanology and Geothermal Research, **106**, 195-210.

Hillhouse, J.W. & Wells, R.E. 1991. Magnetic fabric, flow directions, and source area of the lower Miocene Peach Springs Tuff in Arizona, California, and Nevada. Journal of Geophysical Research, **96**, 12443-12460.

Holness, M. & Humphreys, M. 2003. The Traigh Bhàn na Sgùrra sill, Isle of Mull: Flow localization in a major magma conduit. Journal of Petrology, **44**, 1961-1976.

Horsman, E., Tikoff, B. & Morgan, S. 2005. Emplacement-related fabric and multiple sheets in the Maiden Creek sill, Henry Mountains, Utah, USA. Journal of Structural Geology, **27**, 1426-1444.

Hrouda, F. 1982. Magnetic anisotropy of rocks and its application in geology and geophysics. Geophysical surveys, **5**, 37-82.

Huppert, H.E. & Sparks, R.S.J. 1989. Chilled margins in igneous rocks. Earth and Planetary Science Letters, **92**, 397-405.

Kavanagh, J.L., Menand, T. & Sparks, R.S.J. 2006. An experimental investigation of sill formation and propagation in layered elastic media. Earth and Planetary Science Letters, **245**, 799-813.

King, R. 1966. The magnetic fabric of some Irish granites. Geological Journal, **5**, 43-66.

Kissel, C., Laj, C., Sigurdsson, H. & Guillou, H. 2010. Emplacement of magma in Eastern Iceland dikes: Insights from magnetic fabric and rock magnetic analyses. Journal of Volcanology and Geothermal Research, **191**, 79-92.

Knight, M.D. & Walker, G.P. 1988. Magma flow directions in dikes of the Koolau Complex, Oahu, determined from magnetic fabric studies. Journal of Geophysical Research, **93**, 4301-4319.

Knight, M.D., Walker, G.P., Ellwood, B.B. & Diehl, J.F. 1986. Stratigraphy, paleomagnetism, and magnetic fabric of the Toba Tuffs: constraints on the sources and eruptive styles. Journal of Geophysical Research: Solid Earth (1978–2012), **91**, 10355-10382.

Kratinova, Z., Machek, M. & Kusbach, V. 2010. Fabric transpositions in granite plutons—An insight from non-scaled analogue modelling. Journal Of The Geological Society Of India, **75**, 267-277.

Kuenen, P.H. 1937. Intrusion of Cone-Sheets. Geological Magazine, **74**, 177-183.

Latypov, R.M. 2003. The origin of basic–ultrabasic sills with S-, D-, and I-shaped compositional profiles by in situ crystallization of a single input of phenocryst-poor parental magma. Journal of Petrology, **44**, 1619-1656.

Launeau, P. & Cruden, A. 1998. Magmatic fabric acquisition mechanisms in a syenite: results of a combined anisotropy of magnetic susceptibility and image analysis study. Journal of Geophysical Research, **103**, 5067-5089.

Le Pennec, J.-L., Chen, Y., Diot, H., Froger, J.-L. & Gourgaud, A. 1998. Interpretation of anisotropy of magnetic susceptibility fabric of ignimbrites in terms of kinematic and sedimentological mechanisms: An Anatolian case-study. Earth and Planetary Science Letters, **157**, 105-127.

Liss, D., Hutton, D.H. & Owens, W.H. 2002. Ropy flow structures: A neglected indicator of magma-flow direction in sills and dikes. Geology, **30**, 715-718.

Magee, C. 2011. Emplacement of sub-volcanic cone sheet intrusions. Ph.D Thesis, U**niversity of Birmingham**.

Magee, C. 2012. Incremental emplacement of the sheeted Glas Bheinn Porphyritic Dolerite, Ardnamurchan, NW Scotland. Scottish Journal of Geology, **48**, 119-131.

Magee, C., Stevenson, C., O'Driscoll, B., Schofield, N. & McDermott, K. 2012a. An alternative emplacement model for the classic Ardnamurchan cone sheet swarm, NW Scotland, involving lateral magma supply via regional dykes. Journal of Structural Geology, **43**, 73-91.

Magee, C., Stevenson, C.T.E., O'Driscoll, B. & Petronis, M.S. 2012b. Local and regional controls on the lateral emplacement of the Ben Hiant Dolerite intrusion, Ardnamurchan (NW Scotland). Journal of Structural Geology, **39**, 66-82.

Magee, C., O'Driscoll, B., Petronis, M.S., Stevenson, C.T.E., Clay, P.L. & Gertisser, R. 2013a. Magma Rheology Variations in Sheet Intrusions of the Ardnamurchan Central Complex (Scotland) Inferred from Gabbro Inclusion Characteristics. Journal of Petrology, **54**, 75-102.

Magee, C., Jackson, C.A.-L. & Schofield, N. 2013b. The influence of normal fault geometry on igneous sill emplacement and morphology. Geology, **41**, 407-410.

Magee, C., Jackson, C.L. & Schofield, N. 2014. Diachronous sub-volcanic intrusion along deep-water margins: insights from the Irish Rockall Basin. Basin Research, **26**, 85-105.

Morgan, S., Stanik, A., Horsman, E., Tikoff, B., de Saint Blanquat, M. & Habert, G. 2008. Emplacement of multiple magma sheets and wall rock deformation: Trachyte Mesa intrusion, Henry Mountains, Utah. Journal of Structural Geology, **30**, 491-512.

Muirhead, J.D., Airoldi, G., Rowland, J.V. & White, J.D. 2012. Interconnected sills and inclined sheet intrusions control shallow magma transport in the Ferrar large igneous province, Antarctica. Geological Society of America Bulletin, **124**, 162-180.

O'Driscoll, B. 2006. Magmatic Layering and Magnetic Fabrics in the Palaeogene Carlingford Later Gabbros, Co. Louth, Ireland. Irish Journal of Earth Sciences, **24**, 37-50.

O'Driscoll, B. 2007. The Centre 3 layered gabbro intrusion, Ardnamurchan, NW Scotland. Geological Magazine, **144**, 897-908.

O'Driscoll, B., Troll, V.R., Reavy, R.J. & Turner, P. 2006. The Great Eucrite intrusion of Ardnamurchan, Scotland: Reevaluating the ring-dike concept. Geology, **34**, 189.

O'Driscoll, B., Stevenson, C.T.E. & Troll, V.R. 2008. Mineral Lamination Development in Layered Gabbros of the British Palaeogene Igneous Province: A Combined Anisotropy of Magnetic

Susceptibility, Quantitative Textural and Mineral Chemistry Study. Journal of Petrology, **49**, 1187-1221.

O'Reilly, W. 1984. Rock and mineral magnetism. Blackie Glasgow.

Owens, W. & Bamford, D. 1976. Magnetic, seismic, and other anisotropic properties of rock fabrics. Philosophical Transactions of the Royal Society of London A: Mathematical, Physical and Engineering Sciences, **283**, 55-68.

Palmer, H., Ernst, R. & Buchan, K. 2007. Magnetic fabric studies of the Nipissing sill province and Senneterre dykes, Canadian Shield, and implications for emplacement. Canadian Journal of Earth Sciences, **44**, 507-528.

Parry, L. 1982. Magnetization of immobilized particle dispersions with two distinct particle sizes. Physics of the Earth and Planetary Interiors, **28**, 230-241.

Petronis, M., O'Driscoll, B., Troll, V., Emeleus, C. & Geissman, J. 2009. Palaeomagnetic and anisotropy of magnetic susceptibility data bearing on the emplacement of the Western Granite, Isle of Rum, NW Scotland. Geological Magazine, **146**, 419-436.

Petronis, M.S., Delcamp, A. & van Wyk de Vries, B. 2013. Magma emplacement into the Lemptégy scoria cone (Chaîne Des Puys, France) explored with structural, anisotropy of magnetic susceptibility, and Paleomagnetic data. Bulletin of Volcanology, **75**, 1-22.

Petronis, M.S., Hacker, D.B., Holm, D.K., Geissman, J.W. & Harlan, S.S. 2004. Magmatic flow paths and palaeomagnetism of the Miocene Stoddard Mountain laccolith, Iron Axis region, Southwestern Utah, USA. Geological Society, London, Special Publications, **238**, 251-283.

Phillips, W.J. 1974. The dynamic emplacement of cone sheets. Tectonophysics, **24**, 69-84.

Philpotts, A.R. & Philpotts, D.E. 2007. Upward and downward flow in a camptonite dike as recorded by deformed vesicles and the anisotropy of magnetic susceptibility (AMS). Journal of Volcanology and Geothermal Research, **161**, 81-94.

Planke, S., Rasmussen, T., Rey, S.S. & Myklebust, R. 2005. Seismic characteristics and distribution of volcanic intrusions and hydrothermal vent complexes in the Vøring and Møre basins. In: Doré, A.G. (ed.) Petroleum Geology: North-West Europe and Global Perspectives - Proceddings of the 6th Petroleum Geology Conference. Geological Society, London, 833-844.

Polteau, S., Ferré, E.C., Planke, S., Neumann, E.R. & Chevallier, L. 2008. How are saucer-shaped sills emplaced? Constraints from the Golden Valley Sill, South Africa. Journal of Geophysical Research, **113**, B12104.

Potter, D.K. & Stephenson, A. 1988. Single-domain particles in rocks and magnetic fabric analysis. Geophysical Research Letters, **15**, 1097-1100.

Richey, J.E. & Thomas, H.H. 1930. The Geology of Ardnamurchan, North-West Mull and Coll: A Description of Sheet 51 and Part of Sheet 52 of the Geological Map. Printed under the authority of HM Stationery Office.

Rochette, P. 1987. Magnetic susceptibility of the rock matrix related to magnetic fabric studies. Journal of Structural Geology, **9**, 1015-1020.

Rochette, P. & Fillion, G. 1988. Identification of multicomponent anisotropies in rocks using various field and temperature values in a cryogenic magnetometer. Physics of the Earth and Planetary Interiors, **51**, 379-386.

Rochette, P., Aubourg, C. & Perrin, M. 1999. Is this magnetic fabric normal? A review and case studies in volcanic formations. Tectonophysics, **307**, 219-234.

Sant'Ovaia, H., Bouchez, J., Noronha, F., Leblanc, D. & Vigneresse, J. 2000. Composite-laccolith emplacement of the post-tectonic Vila Pouca de Aguiar granite pluton (northern Portugal): a combined AMS and gravity study. Geological Society of America Special Papers, **350**, 123-137.

Saunders, A., Fitton, J., Kerr, A., Norry, M. & Kent, R. 1997. The north Atlantic igneous province. Large igneous provinces: Continental, oceanic, and planetary flood volcanism, 45-93.

Schirnick, C., van den Bogaard, P. & Schmincke, H.-U. 1999. Cone sheet formation and intrusive growth of an oceanic island—The Miocene Tejeda complex on Gran Canaria (Canary Islands). Geology, **27**, 207-210.

Schofield, N., Heaton, L., Holford, S.P., Archer, S.G., Jackson, C.A.L. & Jolley, D.W. 2012a. Seismic imaging of 'broken bridges': linking seismic to outcrop-scale investigations of intrusive magma lobes. Journal of the Geological Society, **169**, 421-426.

Schofield, N., Stevenson, C. & Reston, T. 2010. Magma fingers and host rock fluidization in the emplacement of sills. Geology, **38**, 63-66.

Schofield, N.J., Brown, D.J., Magee, C. & Stevenson, C.T. 2012b. Sill morphology and comparison of brittle and non-brittle emplacement mechanisms. Journal of the Geological Society, **169**, 127-141.

Schulmann, K. & Ježek, J. 2012. Some remarks on fabric overprints and constrictional AMS fabrics in igneous rocks. International Journal of Earth Sciences, **101**, 705-714.

Siler, D.L. & Karson, J.A. 2009. Three-dimensional structure of inclined sheet swarms: Implications for crustal thickening and subsidence in the volcanic rift zones of Iceland. Journal of Volcanology and Geothermal Research, **188**, 333-346.

Sparks, R., Biggs, J. & Neuberg, J. 2012. Monitoring volcanoes. Science, **335**, 1310-1311.

Sparks, R.S.J. 2003. Forecasting volcanic eruptions. Earth and Planetary Science Letters, **210**, 1-15.

Speight, J., Skelhorn, R., Sloan, T. & Knaap, R. 1982. The dyke swarms of Scotland. Igneous rocks of the British Isles, 449-459.

Stephenson, A. 1994. Distribution anisotropy: two simple models for magnetic lineation and foliation. Physics of the Earth and Planetary Interiors, **82**, 49-53.

Stevenson, C.T.E., Owens, W.H. & Hutton, D.H.W. 2007a. Flow lobes in granite: The determination of magma flow direction in the Trawenagh Bay Granite, northwestern Ireland, using anisotropy of magnetic susceptibility. Geological Society of America Bulletin, **119**, 1368-1386.

Stevenson, C.T.E., Owens, W.H., Hutton, D.H.W., Hood, D.N. & Meighan, I.G. 2007b. Laccolithic, as opposed to cauldron subsidence, emplacement of the Eastern Mourne pluton, N. Ireland: evidence from anisotropy of magnetic susceptibility. Journal of the Geological Society, **164**, 99-110.

Tarling, D. & Hrouda, F. 1993. Magnetic anisotropy of rocks. Springer.

Tauxe, L., Gee, J. & Staudigel, H. 1998. Flow directions in dikes from anisotropy of magnetic susceptibility data: The bootstrap way. Journal of Geophysical Research: Solid Earth (1978–2012), **103**, 17775-17790.

Thomson, K. & Hutton, D. 2004. Geometry and growth of sill complexes: insights using 3D seismic from the North Rockall Trough. Bulletin of Volcanology, **66**, 364-375.

Thomson, K. & Schofield, N. 2008. Lithological and structural controls on the emplacement and morphology of sills in sedimentary basins. In: Thomson, K. & Petford, N. (eds.) Structure and Emplacement of High-Level Magmatic Systems. Geological Society, London, Special Publications, **1**, 31-44.

Tibaldi, A. & Pasquarè, F.A. 2008. A new mode of inner volcano growth: The “flower intrusive structure”. Earth and Planetary Science Letters, **271**, 202-208.

Trubač, J., Žák, J., Chlupáčová, M. & Janoušek, V. 2009. Magnetic fabric of the Říčany granite, Bohemian Massif: A record of helical magma flow? Journal of Volcanology and Geothermal Research, **181**, 25-34.

Walker, G.P.L. 1993. Re-evaluation of inclined intrusive sheets and dykes in the Cuillins volcano, Isle of Skye. In: Prichard, H.M., Alabaster, T., Harris, N.B.W. & Neary, C.R. (eds.) Magmatic Processes and Plate Tectonics. Geological Society, London, Special Publications, **76**, 489-497.

Figure Captions

Figure 1: Schematic diagram of Newtonian magma flow within a sheet intrusion and the imbricated fabrics which may be developed.

Figure 2: Simplified geological map of the Ardnamurchan Central Complex (based on Emeleus 2009) diagrammatically highlighting the attitude of the inclined (cone) sheets and also the locations of the intrusions studied here. Bedding and intrusion dip and strikes omitted for clarity. Location map of Ardnamurchan inset.

Figure 3: (a) Geological map (1:10,000) highlighting the complexity in inclined sheet geometry and orientation (based on Magee et al. 2012a). The positions of S1, S2 and S3 are indicated. See Figure 1 for location. (b) Equal-area stereographic projections for the four AMS sample sites S1a-d. For the average principal susceptibility axes, 95% confidence ellipses are plotted. A schematic depiction of the magnetic fabric imbrication relative to the intrusion plane is also presented.

Figure 4: (a) Field photograph and interpretation of the S1e-h site (note that S1e was drilled on the top surface of the intrusion) and surrounding inclined sheets. See Figure 3a for location and key. (b) Equal-area stereographic projections for the four AMS sample sites S1e-h. For the average principal susceptibility axes, 95% confidence ellipses are plotted. See Figure 3b for key. (c) Plots of P_j against K_{mean} and T for the three defined groupings within the vertical traverse S1h. See Figure 4b for key. (d) A schematic depiction of the magnetic fabric imbrication relative to the intrusion plane.

Figure 5: (a) Field photograph and interpretation of S2, highlighting its ‘ramp-flat’ morphology. (b) Field photograph focusing on the ramp section delineated in Figure 5a. (c) Equal-area stereographic projections for the four AMS sample sites S2a-d. For the average principal susceptibility axes, 95% confidence ellipses are plotted. See Figure 3b for key. (d) Plot of P_j versus T for S2a-d. (e) Schematic representation of the orientation of the S2a-c magnetic fabrics within the ramp portion of S2.

Figure 6: Equal-area stereographic projections for the three AMS sample sites S2e-g. For the average principal susceptibility axes, 95% confidence ellipses are plotted. See Figure 3b for key and Figure 5a for sample location.

Figure 7: Anisotropy of magnetic susceptibility data and sample positions for the two S3 sites. The individual specimen locations in (a) and (b) correspond to S3b and S3e, respectively. Sketches of the fabric imbrication relative to the intrusion plane are also shown.

Figure 8: (a and b) Field photograph and interpretation of the S4 and surrounding inclined sheets. See Figure 1 for location. (c) Equal-area stereographic projections for the six AMS sample sites S4a-f. For the average principal susceptibility axes, 95% confidence ellipses are plotted. The orientation (163–343°; grey arrow) of an intrusive step observed near S4a-c is incorporated. See Figure 3b for key. The principal susceptibility axes marked in grey on the S4d stereoplot correspond to sample CSJ1, which was collected from the same site, from Magee et al. (2012a).

Figure 9: Sketch of S5 highlighting the location of the four AMS profiles sampled and their corresponding equal-area stereographic projections. For the average principal susceptibility axes, 95% confidence ellipses are plotted. See Figure 3b for key.

Figure 10: Equal-area stereographic projections for the six AMS sample sites S6a-d. For the average principal susceptibility axes, 95% confidence ellipses are plotted. The orientation (158–338°; grey arrow) of an intrusive step observed near S6a-c is incorporated. See Figure 3b for key.

Figure 11: (a and b) Aerial view of S7 depicting the elongated segments. Sample sites and inferred magma flow patterns are also marked on (a). Note the monoclinal folding of the olivine-basal lavas (thick black lines). See Figure 1 for location. (c) Field photograph and interpretation of the S7d highlighting the along strike variation in thickness and possible definition of magma fingers. (d) Equal-area stereographic projections for the four AMS sample sites S7a-d. For the average principal susceptibility axes, 95% confidence ellipses are plotted. The grey arrows denote the elongation direction of the samples respective lobe. Stars distinguish the intrusion poles. See Figure 3b for key.

Figure 12: (a-d) Low-temperature versus susceptibility plots for S3b, S3f, S4c, and S5b. Arrows demarcate the Curie Point. (e) Day Plot of hysteresis parameters (ratio of saturation remanence to saturation magnetization Mrs/Ms and the ratio of remanent coercive force to ordinary coercive force Hcr/Hc. The relationship between Mrs/Ms and Hcr/Hc defines the magnetic grain size of the ferromagnetic phase (single-domain (SD), pseudo-single-domain (PSD), and multidomain (MD)). All data for the Ardnamurchan inclined sheets plot in the PSD field on the Day plot (Day et al. 1977; Parry 1982).

Figure 13: (a) Schematic diagram of an intrusive segment bounded by steps and the possible internal magma flow profile generated by high velocity gradients (greyscale) at the top and lower contacts as well as the lateral step boundaries for magmas with Newtonian or Bingham rheologies (modified from Magee et al. 2013a). (b) The lobe geometry created produces a range of measurable fabric orientations, including apparent differences in imbrication closure directions. This indicates that sample location may play a pivotal role on controlling the measured fabrics.

Figure 14: Geological map of Ardnamurchan highlighting magma flow axes inferred from AMS (this study; Magee et al. 2012a). Two potential magma flow orientations are shown for S1 (see text). See Figures 2 and 3A for key.

TABLE 1. AMS RESULTS

AMS profile	No. of spec.	K_{mean} (10^{-2}) (SI)	K_1 Dec. (°)	Pl. (°)	K_2 Dec. (°)	Pl. (°)	K_3 Dec. (°)	Pl. (°)	Mag. fol. Str. (°)	Dip (°)	P_j	T	Inclined sheet Str. (°)	Dip (°)	Dip dir.
S1*a*	21	3.03	316	03	226	08	063	81	153	09	1.025	-0.839	129	18	SW
S1*b*	10	5.11	136	26	010	51	240	27	150	63	1.046	-0.721	129	18	SW
S1*c*	05	4.79	134	25	345	61	231	13	141	77	1.038	-0.028	129	18	SW
S1*d*	12	5.50	134	29	011	44	244	32	154	58	1.038	-0.602	129	18	SW
S1*e*	24	6.16	142	09	235	18	026	70	116	20	1.039	-0.169	142	15	SW
S1*f*	28	6.91	128	03	302	60	037	03	127	88	1.026	-0.619	142	15	SW
S1*g*	13	6.29	138	14	228	00	319	76	049	14	1.036	-0.522	142	15	SW
S1*h_A*	05	6.51	138	25	046	05	304	65	034	25	1.028	-0.495	142	15	SW
S1*h_B*	10	7.15	147	23	033	45	255	36	165	54	1.024	-0.450	142	15	SW
S1*h_C*	25	6.98	113	45	326	41	220	17	130	73	1.024	-0.069	142	15	SW
S2*a*	13	4.13	319	17	229	00	139	73	049	17	1.017	0.358	048	44	NW
S2*b*	16	5.33	126	15	029	25	244	60	154	30	1.015	-0.819	048	44	NW
S2*c*	19	5.32	128	04	221	34	032	56	122	34	1.015	-0.705	048	44	NW
S2*d*	13	5.40	134	09	227	21	021	67	111	23	1.014	-0.181	154	10	SW
S2*e*	14	1.93	350	01	080	20	257	70	167	20	1.011	-0.713	161	18	SW
S2*f*	21	1.75	166	00	076	75	256	15	166	75	1.017	-0.243	161	18	SW
S2*g*	21	1.62	342	02	077	73	252	17	162	73	1.016	-0.670	161	18	SW
S3*a*	19	4.91	144	26	336	63	237	05	147	85	1.068	0.792	152	90	-
S3*b*	19	5.21	049	88	159	01	249	02	159	88	1.073	0.579	152	90	-
S3*c*	15	4.92	148	74	346	16	255	05	165	85	1.065	0.488	152	90	-
S3*d*	15	5.21	272	77	139	09	048	09	138	81	1.028	0.049	152	90	-
S3*e*	53	5.22	128	77	338	12	247	07	157	83	1.030	0.256	152	90	-
S3*f*	19	5.90	122	81	332	07	241	06	151	84	1.039	0.087	152	90	-
S4*a*	24	3.57	155	72	323	18	054	04	144	86	1.027	-0.706	038	07	W
S4*b*	12	4.15	315	40	165	46	058	15	148	75	1.031	-0.361	038	07	W
S4*c*	06	2.59	321	59	207	14	109	27	019	63	1.020	-0.736	038	07	W
S4*d*	17	3.40	355	48	182	42	089	03	179	87	1.019	-0.109	035	58	W
S4*e*	26	3.52	317	33	116	56	221	10	131	80	1.029	-0.600	020	46	W
S4*f*	17	2.57	327	43	076	19	183	41	093	49	1.015	-0.594	020	46	W
S5*a*	16	4.65	159	02	268	84	069	06	159	84	1.022	0.316	042	22	N
S5*b*	26	3.33	151	06	057	40	248	50	158	40	1.026	-0.460	042	22	N
S5*c*	13	3.65	128	17	028	29	244	55	154	35	1.009	-0.219	042	22	N
S5*d*	77	4.24	152	27	006	58	250	15	160	75	1.029	-0.167	042	22	N
S6*a*	19	5.28	355	21	087	04	188	69	098	21	1.031	0.006	096	30	N
S6*b*	24	3.68	349	11	081	10	212	75	122	15	1.043	0.048	096	30	N
S6*c*	15	5.22	343	23	076	07	182	66	092	24	1.026	-0.043	096	30	N
S6*d*	26	4.91	354	20	088	10	203	68	113	22	1.037	0.142	096	30	N
S7*a*	25	3.68	144	44	262	26	012	35	102	55	1.033	0.339	037	30	WNW
S7*b*	20	6.87	171	58	270	06	004	31	094	59	1.141	0.587	074	30	NW
S7*c*	24	5.79	107	67	341	14	247	18	157	72	1.049	-0.096	080	03	N
S7d	33	3.64	141	32	332	57	234	05	144	85	1.019	-0.270	058	30	N

Figure 1

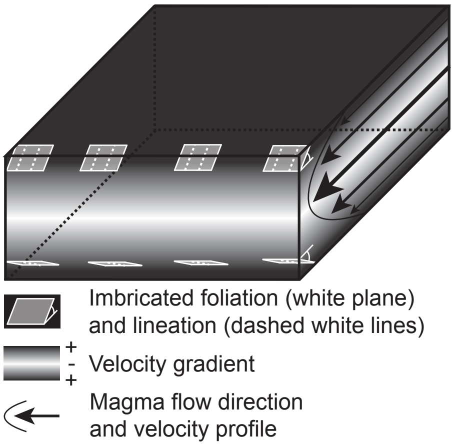
Imbricated foliation (white plane)
and lineation (dashed white lines)
+
-
+
Velocity gradient
Magma flow direction
and velocity profile

Figure 2

Figure 2

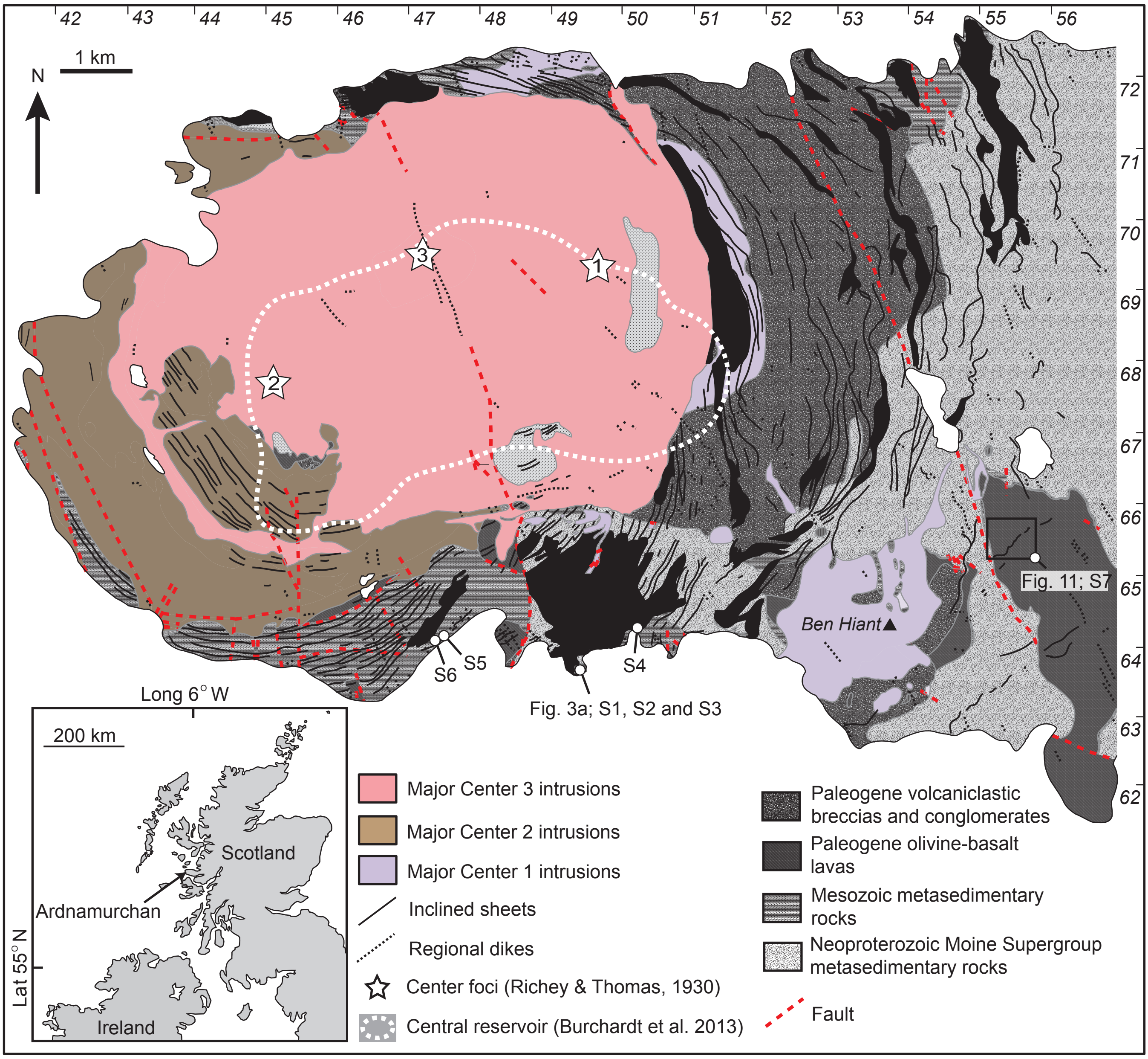

Figure 3

Figure 3

Click here to download Figure Fig. 3 - Mingary map and S1a-d.pdf

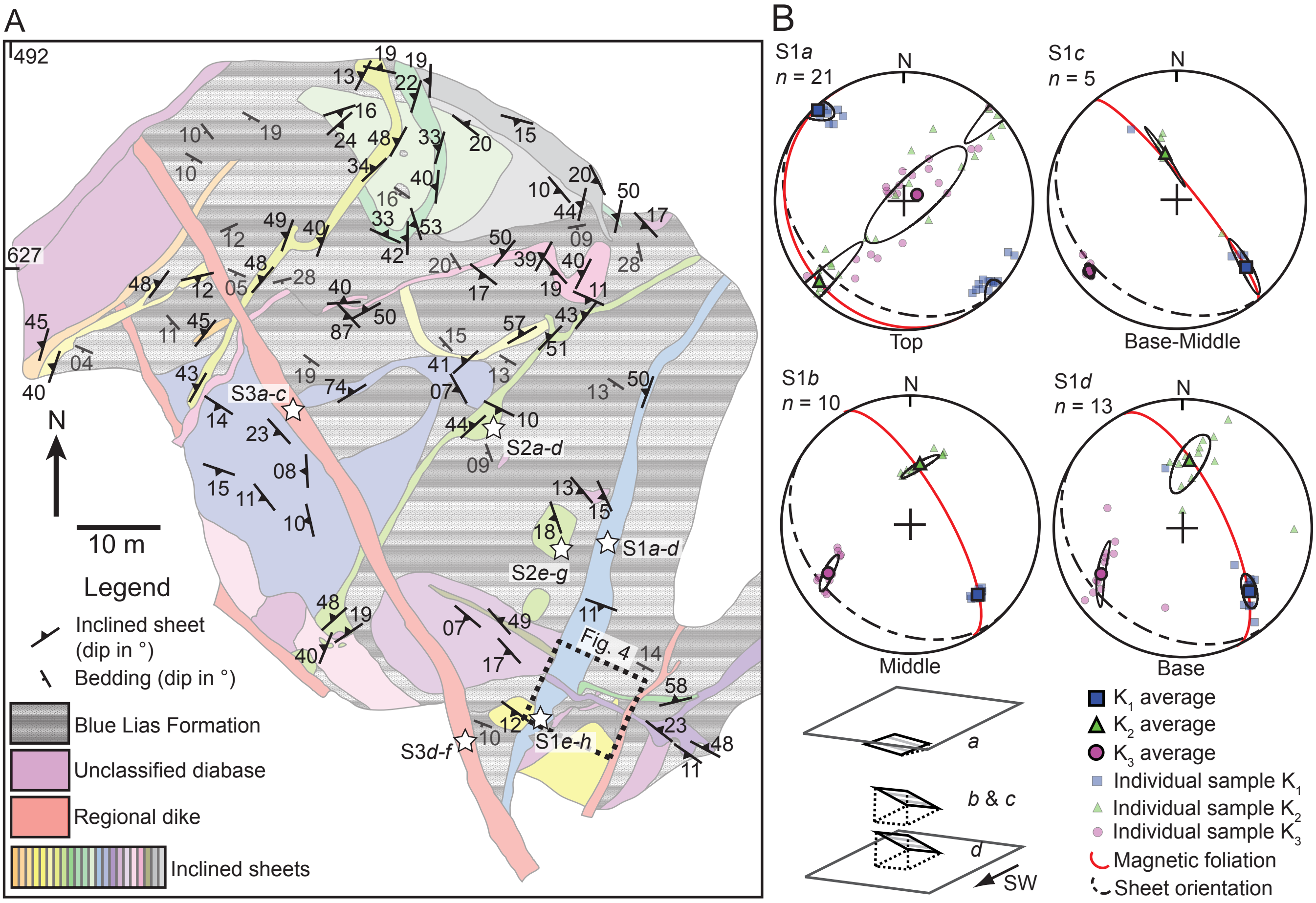

Figure 4

Figure 4

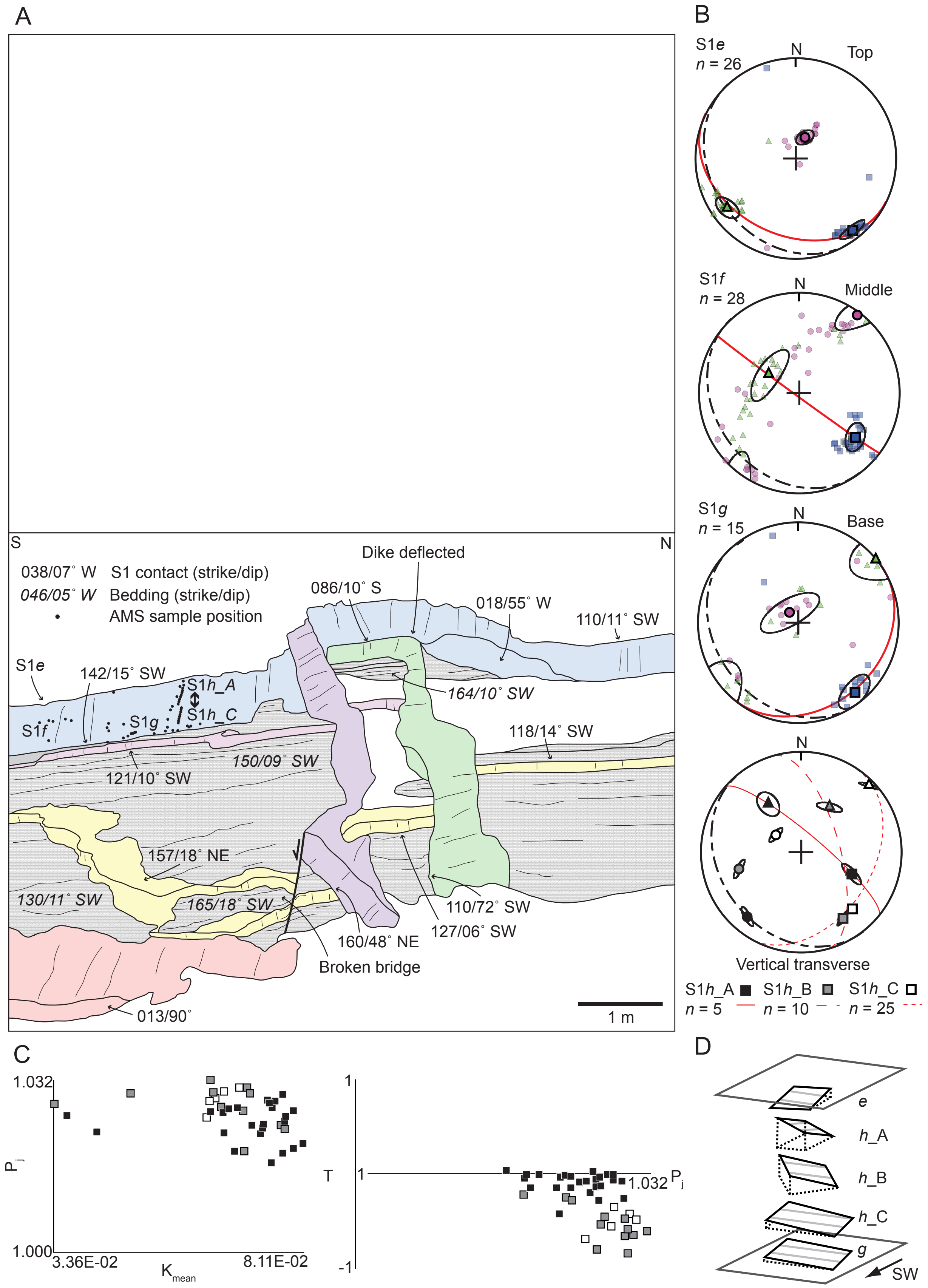

Figure 5

Figure 5

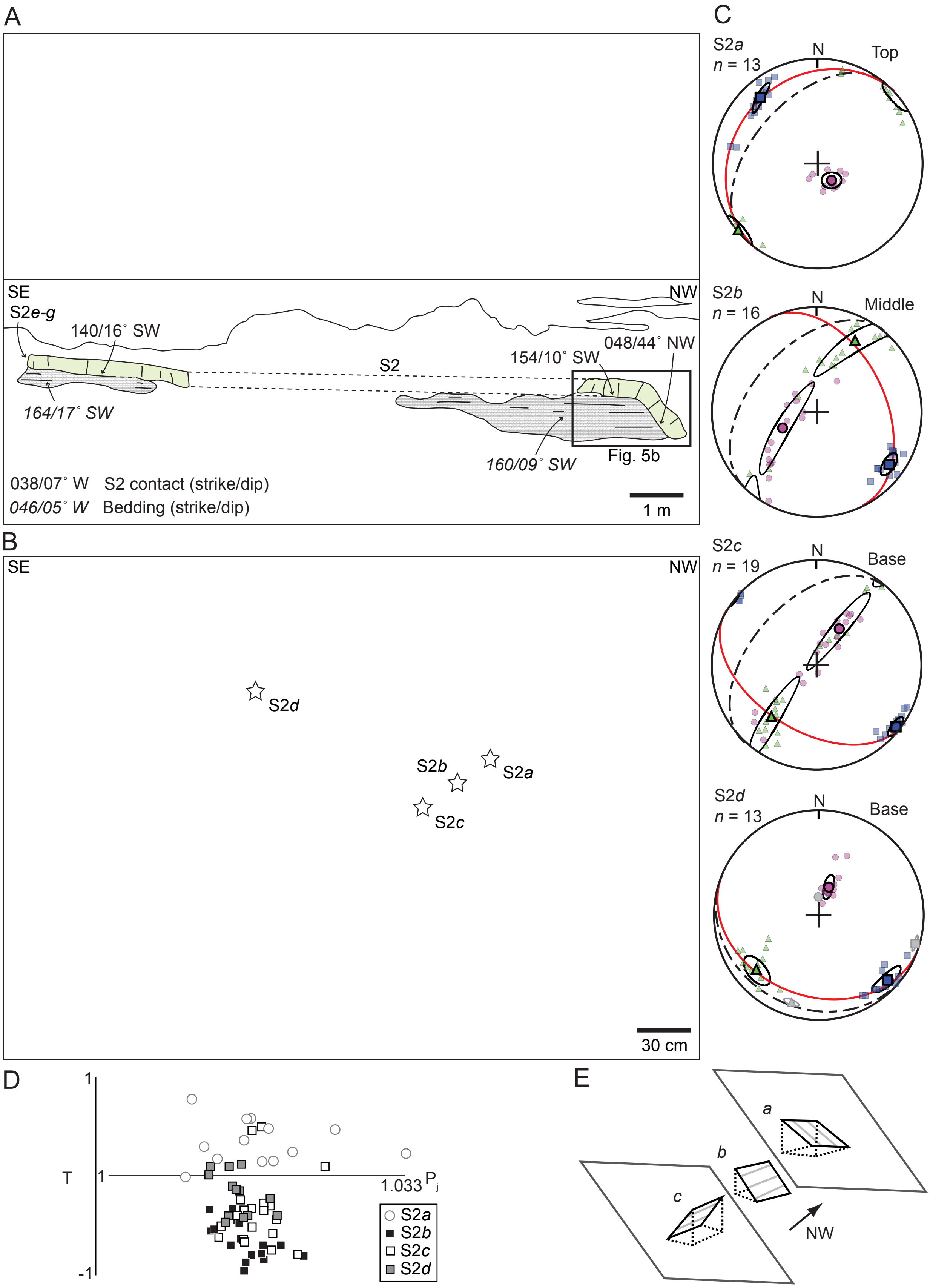

Figure 6

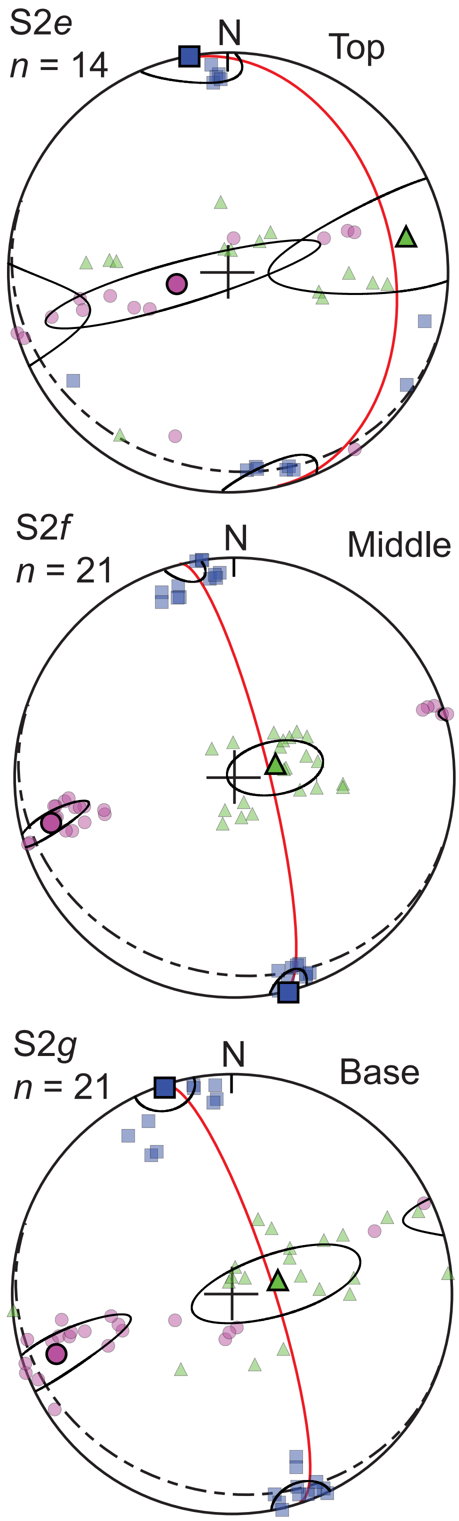

Figure 7

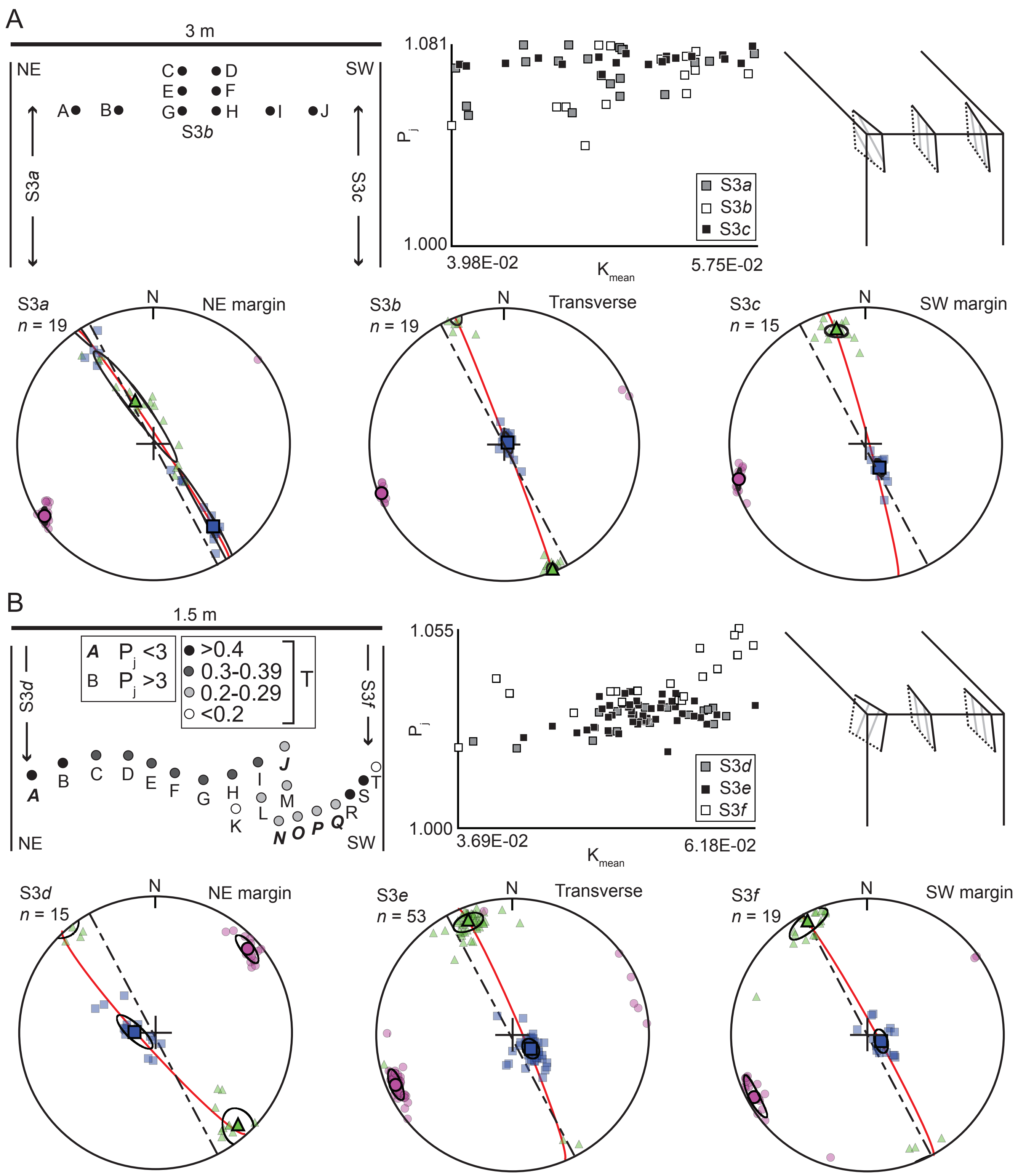
A
3 m
NE
SW
C
D
E
F
G
H
A
B
I
J
S3b
S3a
S3c
1.081
1.000
Pj
3.98E-02
Kmean
5.75E-02
S3a
S3b
S3c
S3a
n = 19
N
NE margin
S3b
n = 19
N
Transverse
S3c
n = 15
N
SW margin
B
1.5 m
A Pj <3
B Pj >3
>0.4
0.3-0.39
0.2-0.29
<0.2
T
S3d
S3f
NE
SW
A
B
C
D
E
F
G
H
I
J
K
L
M
N
O
P
Q
R
S
T
1.055
1.000
Pj
3.69E-02
Kmean
6.18E-02
S3d
S3e
S3f
S3d
n = 15
N
NE margin
S3e
n = 53
N
Transverse
S3f
n = 19
N
SW margin

Figure 8

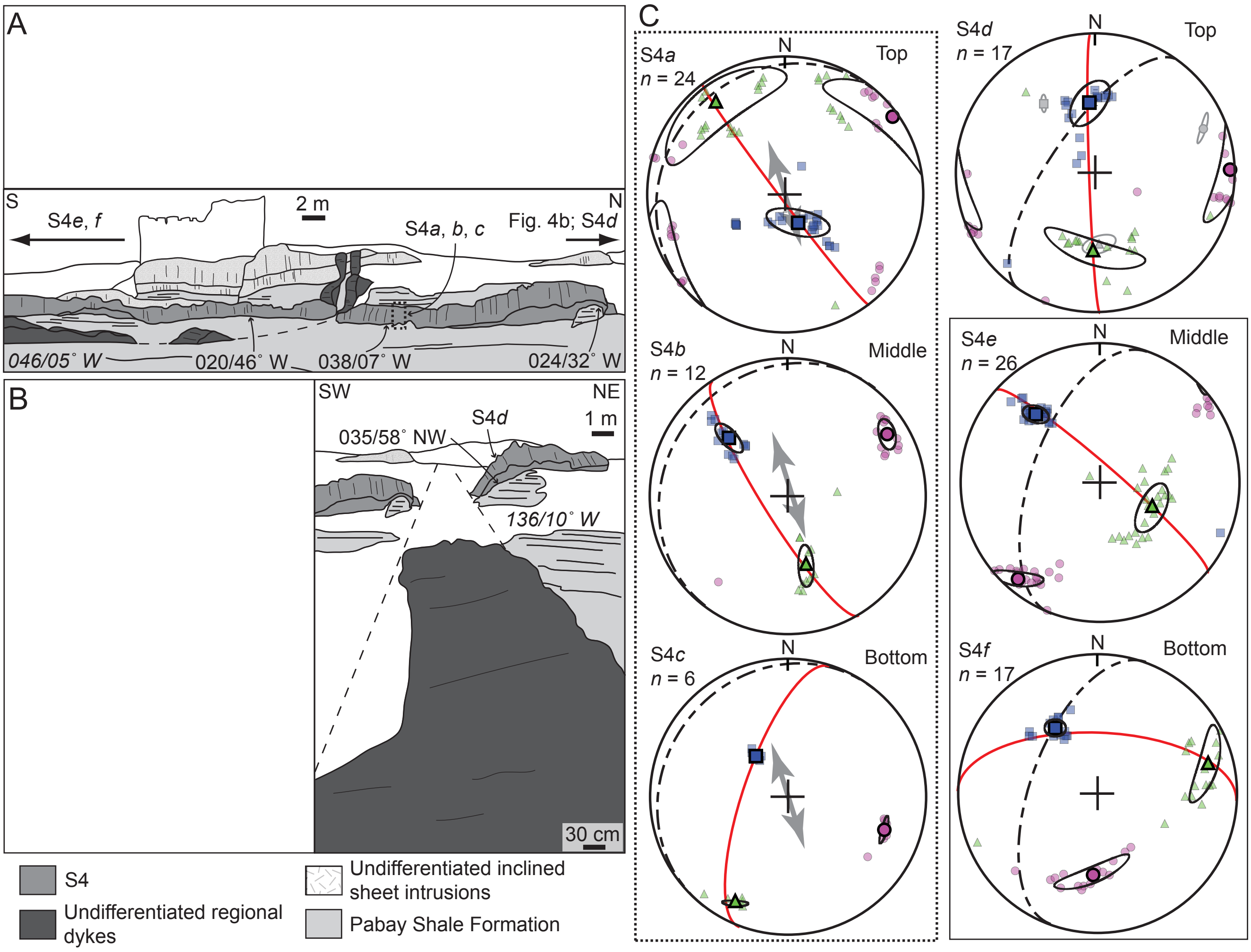
A
S
N
S4e, f
2 m
S4a, b, c
Fig. 4b; S4d
046/05° W
020/46° W
038/07° W
024/32° W
B
SW
NE
S4d
1 m
035/58° NW
136/10° W
30 cm
S4
Undifferentiated regional dykes
Undifferentiated inclined sheet intrusions
Pabay Shale Formation
C
S4a
n = 24
Top
S4b
n = 12
Middle
S4c
n = 6
Bottom
S4d
n = 17
Top
S4e
n = 26
Middle
S4f
n = 17
Bottom
N

Figure 9 Click here to download Figure Fig. 9 - S5 new.pdf

Figure 9

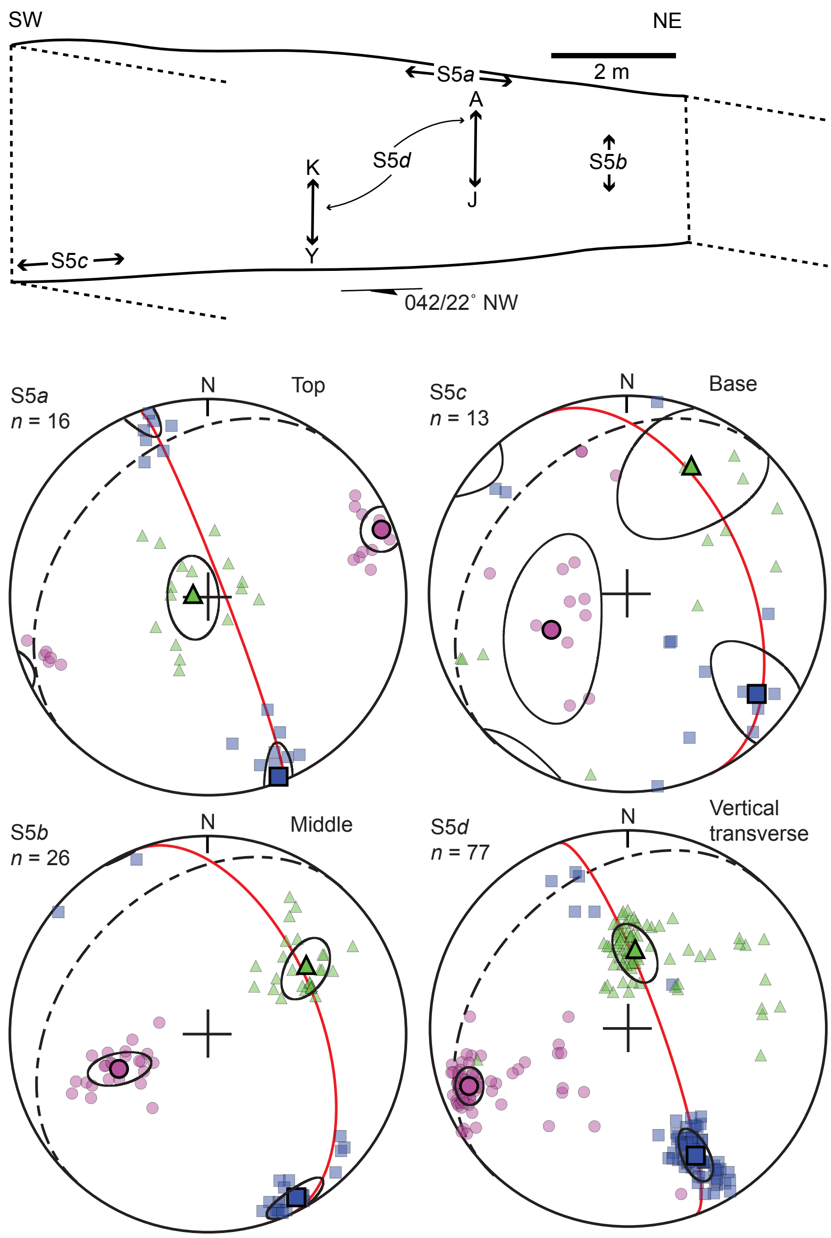

Figure 10

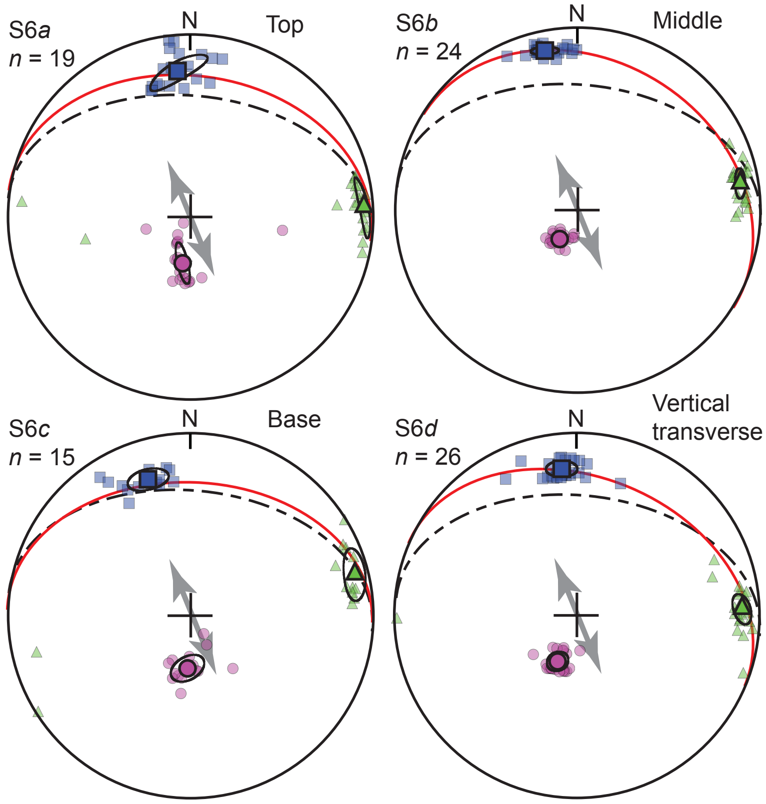
S6a
n = 19
N
Top
S6b
n = 24
N
Middle
S6c
n = 15
N
Base
S6d
n = 26
N
Vertical
transverse

Figure 11

Figure 11

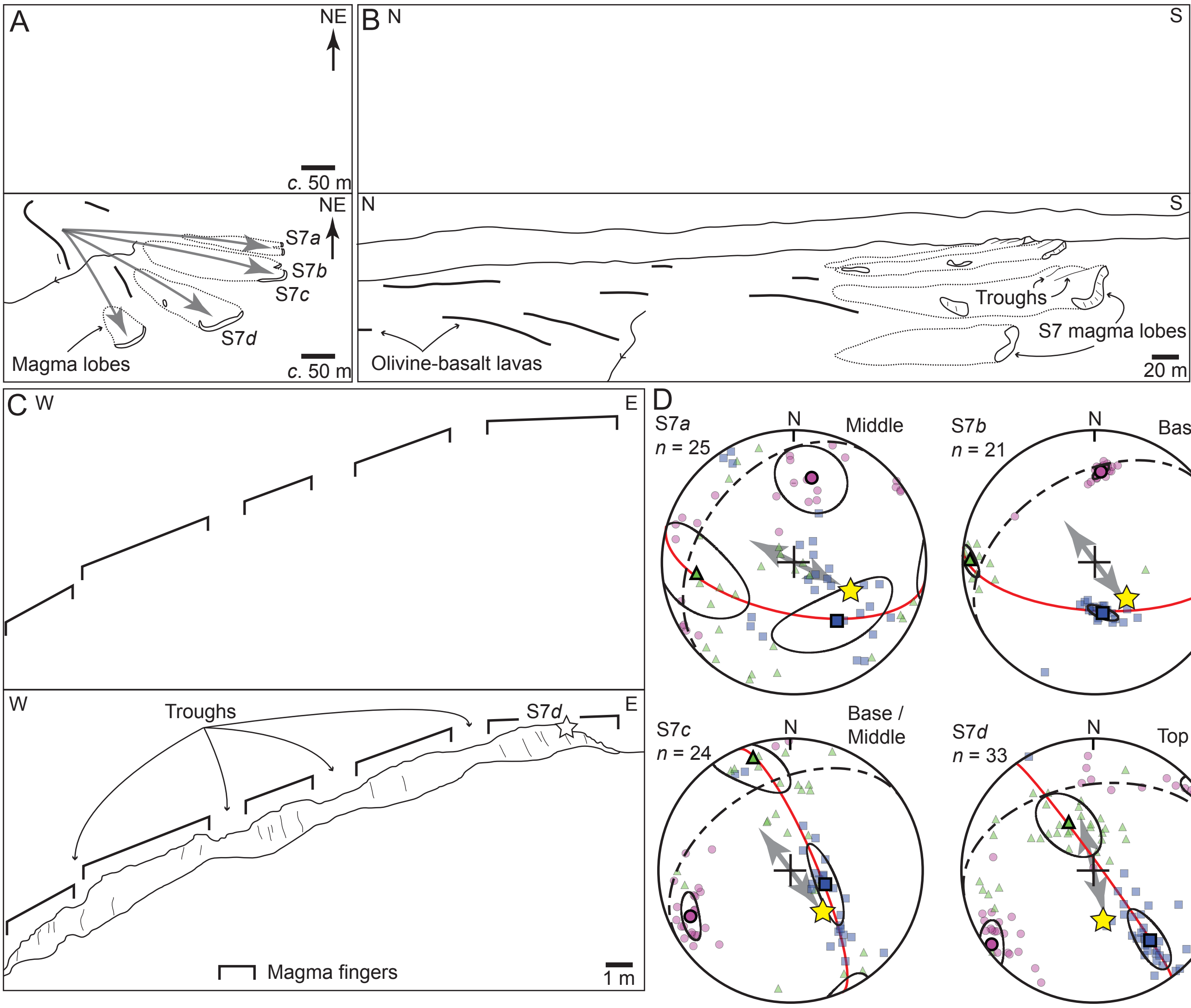

Figure 12

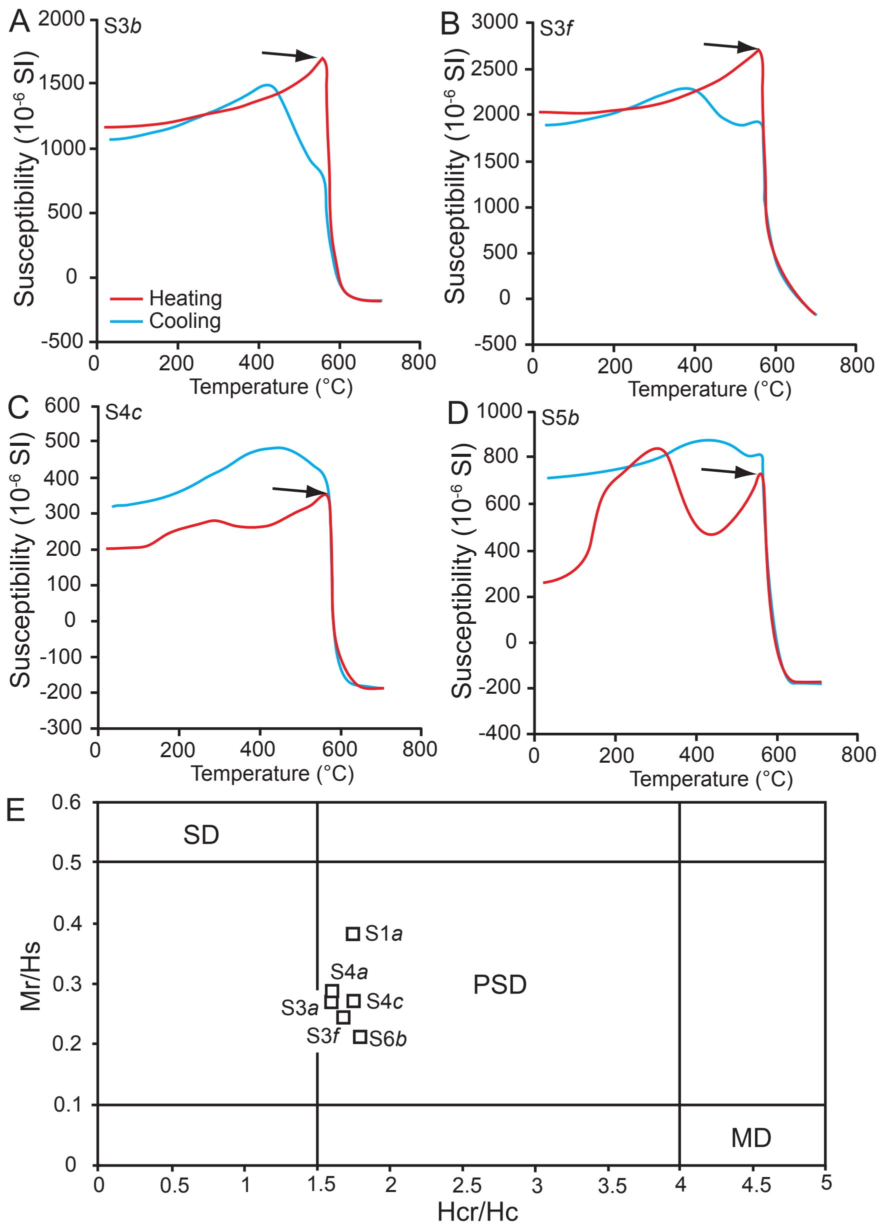
A
S3b
Susceptibility (10^-6 SI)
Heating
Cooling
Temperature (°C)
B
S3f
C
S4c
D
S5b
E
SD
PSD
MD
S1a
S4a
S3a
S4c
S3f
S6b
Mr/Hs
Hcr/Hc

Figure 13

Figure 13

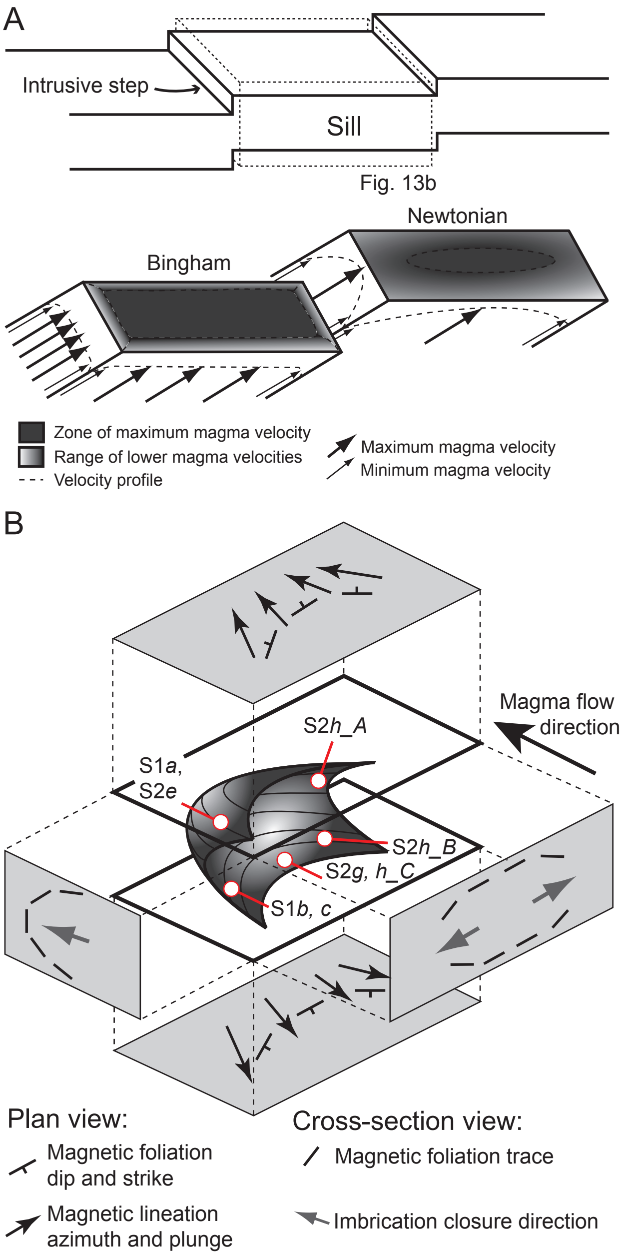

Figure 14

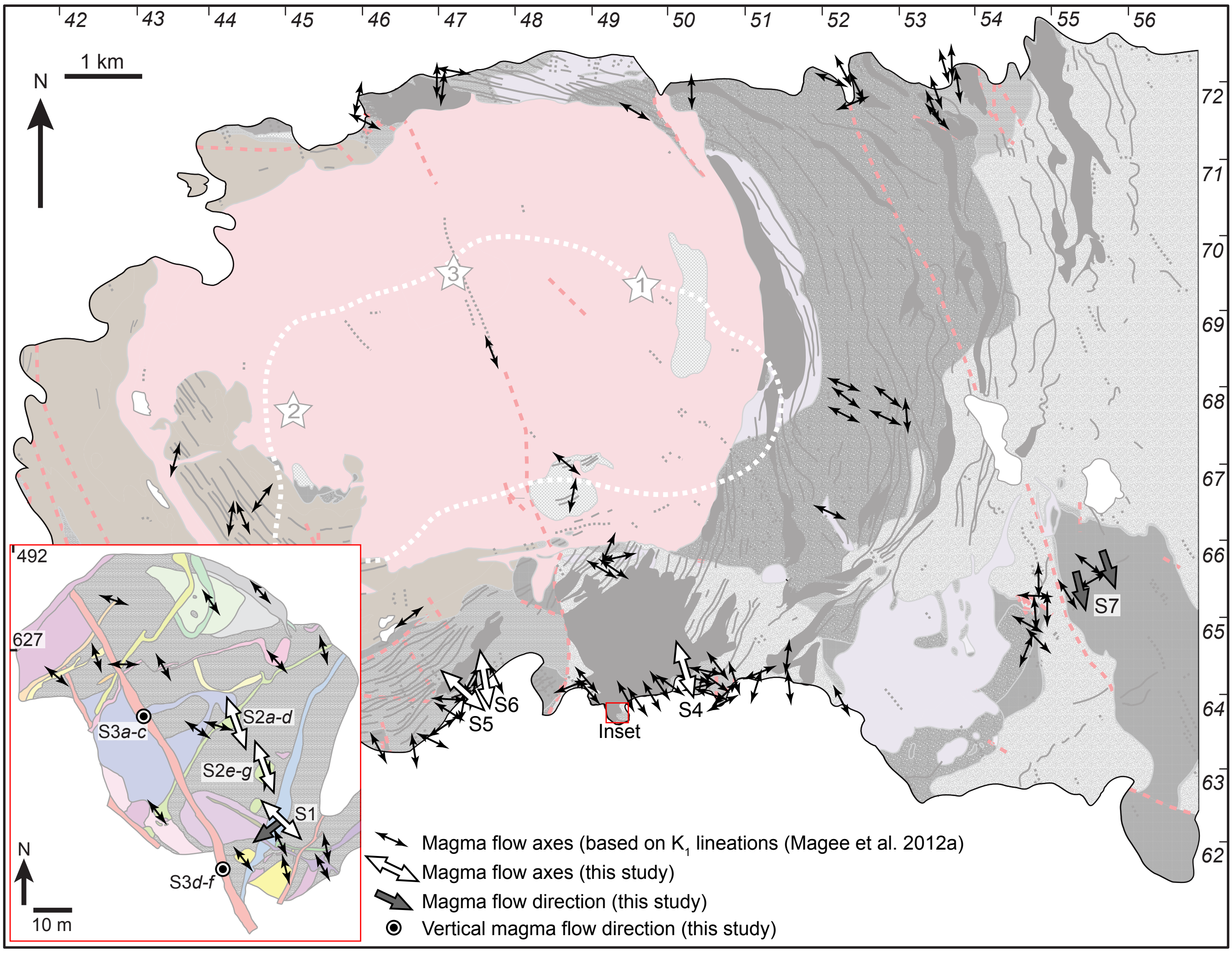

1 km
N
42
43
44
45
46
47
48
49
50
51
52
53
54
55
56
72
71
70
69
68
67
66
65
64
63
62
S4
S5
S6
S7
Inset
492
627
S3a-c
S2a-d
S2e-g
S1
S3d-f
N
10 m
Magma flow axes (based on K1 lineations (Magee et al. 2012a)
Magma flow axes (this study)
Magma flow direction (this study)
Vertical magma flow direction (this study)